

**SYNTHETIC APERTURE RADAR PROCESSING USING UWB
OFDM SIGNALS**

BY

MOHAMMED DAHIRU BUHARI

A Thesis Presented to the
DEANSHIP OF GRADUATE STUDIES

KING FAHD UNIVERSITY OF PETROLEUM & MINERALS
DHAHRAN, SAUDI ARABIA

In Partial Fulfillment of the
Requirements for the Degree of

MASTER OF SCIENCE


In

ELECTRICAL ENGINEERING

MARCH 2014

KING FAHD UNIVERSITY OF PETROLEUM & MINERALS
DHAHRAN- 31261, SAUDI ARABIA
DEANSHIP OF GRADUATE STUDIES

This thesis, written by MOHAMMED DAHIRU BUHARI under the direction of his thesis advisor and approved by his thesis committee, has been presented and accepted by the Dean of Graduate Studies, in partial fulfillment of the requirements for the degree of **MASTER OF SCIENCE IN TELECOMMUNICATION ENGINEERING.**



Dr. Ali Al-Shaikhi
Department Chairman



Dr. Salam A. Zummo
Dean of Graduate Studies

2/4/14
Date



Dr. Ali Hussein Muqabel
(Advisor)



Dr. Mohamed Adnan Landolsi
(Member)



Dr. Wajih A. Abu Al-Saud
(Member)

© Mohammed Dahiru Buhari

2014

*This work is dedicated to my beloved parents Alhaji Dahiru Hassan & Hajiya
Aishatu Dahiru Hassan.*

ACKNOWLEDGMENTS

Alhamdulillah, all praise be to Allah and peace and blessing be upon his prophet Muhammad (S.A.W). My sincere gratitude to Allah for given me the strength, health and ability to carry out this research. I thank Him for making it possible for me to get the scholarship to study at KFUPM under high ranking faculties that open my eyes into the world of research.

After that, I would like to acknowledge the contributions of my parents. They provided me with the moral and financial assistance needed as an instrument for my academic excellence throughout my life. They are in every aspect of my life making sure that I succeed.

My profound gratitude to my advisor in person of Dr. Ali Hussein Muqaibel for his understanding, concern, constructive criticisms and untiring supervision of the work. I would also like to thank my thesis committee members: Dr. Mohamed Adnan Landolsi and Dr. Wajih A. Abu Al-Saud for their guidance, comments, recommendations and criticisms of the work to see that I produce a qualitative work.

It would be really improper without mentioning the names of my fellow KFUPM colleagues whose moral and emotional support helped me a lot. A few of them are Damilola Sadiq Owudunni, Alam Zaid and Saleh Al Awash. To all the rest; I express my profound gratitude and sincere thanks. To my brothers, sisters and my wife, I reserve all my prayers and good wishes for them. I would also like to thank the KFUPM Nigerian community for making me fill at home throughout my stay in the school.

TABLE OF CONTENTS

ACKNOWLEDGMENTS	V
TABLE OF CONTENTS	VI
LIST OF TABLES	X
LIST OF FIGURES	XI
LIST OF ABBREVIATIONS	XIV
LIST OF VARIABLES.....	XVI
ABSTRACT.....	XX
ABSTRACT (ARABIC)	XXI
CHAPTER 1 INTRODUCTION.....	1
1.1 Introduction.....	1
1.2 Thesis Organization	3
1.3 Thesis Contributions	3
CHAPTER 2 TECHNICAL BACKGROUND AND LITERATURE REVIEW.....	5
2.1 Introduction.....	5

2.2	Technical Background	5
2.2.1	Concept of Synthetic Aperture Radar	5
2.2.2	Radar Terminology	7
2.2.3	Radar Functions	10
2.2.4	Basic Principle of OFDM	10
2.2.5	UWB Technology	12
2.2.6	Matched Filtering in SAR	14
2.2.7	Benefits of UWB OFDM SAR System	15
2.3	Literature Review.....	16
2.3.1	High Resolution SAR and OFDM SAR	16
2.3.2	OFDM Waveform Design for Range Ambiguity Suppression.....	19
2.4	Research Motivation	21
2.5	Chapter Summary	22
CHAPTER 3 OFDM SAR CROSS RANGE RECONSTRUCTION.....		23
3.1	Introduction.....	23
3.2	Single Target Cross Range Reconstruction	23
3.2.1	SAR System Geometric Model.....	23
3.2.2	Transmit/Receive Signal Models	25
3.2.3	Phase History Estimate Using Least Square Method	26
3.2.4	Cross Range Profile Reconstruction	29
3.2.5	Simulation and Results	31
3.3	Multiple Targets Cross Range Reconstruction	39
3.3.1	Multiple Target SAR geometry	40
3.3.2	Range Resolution.....	41
3.3.3	Cross Range Resolution.....	42
3.3.4	Simulation and Results	43

3.4 Chapter Summary	48
CHAPTER 4 SAR IMAGE RECONSTRUCTION.....	49
4.1 Introduction.....	49
4.2 Range Imaging	49
4.3 Range Migration Correction (RMC).....	52
4.4 SAR Imaging	54
4.5 Simulation and Results	57
4.5.1 Single Target Imaging.....	57
4.5.2 Multiple Targets Imaging	59
4.6 Chapter Summary	67
CHAPTER 5 OFDM WAVEFORM DESIGN FOR RANGE AMBIGUITY SUPPRESSION.....	68
5.1 Introduction.....	68
5.2 Factors Affecting the Choice of OFDM Signal Vector \mathbf{S}	68
5.3 Impact of Choosing \mathbf{S} Randomly.....	69
5.4 Adaptive Design of OFDM subcarrier N	70
5.5 Design of OFDM Waveform in Range Ambiguity Suppression	71
5.5.1 Uniform/Random Coding	72
5.5.2 Pseudo-Noise (PN) Sequences.....	76
5.5.3 Gold Sequences.....	78
5.5.4 Kasami Sequences	80
5.6 Chapter Summary	83

CHAPTER 6 SUMMARY AND CONCLUSIONS.....	84
6.1 Conclusions.....	84
6.2 Future work.....	86
REFERENCES.....	87
VITAE.....	91

LIST OF TABLES

Table 5.1 Possible Combinations of α and β	73
Table 5.2 Preferred pairs of PN sequences to generate Gold sequence.....	79
Table 5.3 Values of the codes used for the simulation	83

LIST OF FIGURES

Figure 2.1 Example of an image formation in SAR	7
Figure 2.2 PRI and PRF	8
Figure 2.3 SAR imaging (a) Before RMC (b) After RMC	9
Figure 2.4 OFDM modulation techniques	11
Figure 2.5 FCC ruling for UWB spectrum overlay	13
Figure 2.6 UWB behavior in frequency and time domain.....	13
Figure 2.7 Matched Filtering in SAR	15
Figure 3.1 Single target system model.....	24
Figure 3.2 Summary of the procedure of a single target cross range reconstruction.....	30
Figure 3.3 Uniform assignment of the N sub-bands (a) Cross range target position estimation. (b) Cumulative side-lobe level (c) Main lobe width	33
Figure 3.4 Random assignment of the N sub-bands (a) Cross range target position estimation. (b) Cumulative side-lobe level (c) Main lobe width	34
Figure 3.5 Normalized Cross range profile for (a) $N = 4$. (b) $N = 8$. (c) $N = 16$	36
Figure 3.6 Grid search for $N= 4$. (a) Cross range target position estimation(b) Cumulative side-lobe level.	38
Figure 3.7 Grid search for $N= 8$. (a) Cross range target position estimation(b) Cumulative side-lobe level.	38
Figure 3.8 Grid search for $N= 16$. (a) Cross range target position estimation (b) Cumulative side-lobe level.	39
Figure 3.9 System model for two targets scenarios	40
Figure 3.10 Variation of range resolution with bandwidth.....	42
Figure 3.11 Cross range profile for the case of two targets when $dC < \delta x$	44
Figure 3.12 Cross range profile for the case of multiple targets when $dC < \delta x$	45
Figure 3.13 Cross range profile for the case of two targets when $dC \geq \delta x$	46
Figure 3.14 Cross range profile for the case of multiple targets when $dC \geq \delta x$	47
Figure 4.1 SAR Range Imaging.....	50
Figure 4.2 SAR Imaging before RMC	51

Figure 4.3 SAR Cross range Imaging	52
Figure 4.4 SAR Imaging after RMC	54
Figure 4.5 Formation of a 2D SAR Image.....	56
Figure 4.6 2D SAR Imaging for (a) Image before RMC. (b) Image after RMC (c) Final Image.....	58
Figure 4.7 2D SAR Image for two targets scenario when $dC < \delta x$ and $dR < \Delta R$ for (a) Image before RMC. (b) Image after RMC. (c) Final Image.	60
Figure 4.8 2D SAR Image for multiple targets scenario when $dC < \delta x$ and $dR < \Delta R$	61
Figure 4.9 2D SAR Image for two targets scenario when $dC < \delta x$ and $dR \geq \Delta R$ for (a) Image before RMC. (b) Image after RMC. (c) Final Image.	62
Figure 4.10 2D SAR Image for two targets scenario when $dC \geq \delta x$ and $dR < \Delta R$ for (a) Image before RMC. (b) Image after RMC. (c) Final Image.	63
Figure 4.11 2D SAR Image for multiple targets scenario when $dC \geq \delta x$ and $dR < \Delta R$ for (a) Image before RMC. (b) Image after RMC. (c) Final Image.....	64
Figure 4.12 2D SAR Image for two targets scenario when $dC \geq \delta x$ and $dR \geq \Delta R$ for (a) Image before RMC. (b) Image after RMC. (c) Final Image.	65
Figure 4.13 2D SAR Image for multiple targets scenario when $dC \geq \delta x$ and $dR \geq \Delta R$ for (a) Image before RMC. (b) Image after RMC. (c) Final Image.....	66
Figure 5.1 RMSE for (a) Uniform assignment of the sub-bands. (b) Random assignment of the sub-bands.	70
Figure 5.2 RMSE for Uniform assignment of the sub-bands with Adaptive N	71
Figure 5.3 2D SAR Imaging for full random assignment of the sub-bands(a) Image before RMC. (b) Image after RMC. (c) Final Image.	74
Figure 5.4 2D SAR Imaging for uniform/random assignment of the sub-bands(a) Image before RMC. (b) Image after RMC. (c) Final Image for single target (d) Final Image for two targets.	75
Figure 5.5 Transmission and reception process using PN Sequences.	77
Figure 5.6 Generation of a Gold Sequences	79
Figure 5.7 2D SAR Imaging using Gold codes (a) Image before RMC. (b) Image after RMC. (c) Final Image for single target. (d) Final Image for two targets.	81
Figure 5.8 2D SAR Imaging using Kasami codes (a) Image before RMC. (b) Image after	

RMC. (c) Final Image for single target. (d) Final Image for two targets. 82

LIST OF ABBREVIATIONS

ACF	:	Auto Correlation Function
AD	:	Analog to Digital
AWGN	:	Additive White Gaussian Noise
CCF	:	Cross Correlation Function
CDMA	:	Code Division Multiple Access
CS	:	Compressed Sensing
DFT	:	Discrete Fourier Transform
DSP	:	Digital Signal Processing
FM-CW	:	Frequency Modulated Compact Wave
IDFT	:	Inverse Discrete Fourier Transform
IEEE	:	Institute of Electrical Electronics Engineering
ISI	:	Inter Symbol Interference
LFM	:	Linear Frequency Modulation
LSE	:	Least Square Estimation
MIMO	:	Multiple Input Multiple Output
OFDM	:	Orthogonal Frequency Division Multiplexing
PM	:	Phase Modulation
PN	:	Pseudo Noise
PRF	:	Pulse Repetition Frequency

PRI	:	Pulse Repetition Interval
RAR	:	Real Aperture Radar
RCMC	:	Range Cell Migration Correction
RF	:	Radio Frequency
RMSE	:	Root Mean Square Error
RPR	:	Range Profile Reconstruction
SAR	:	Synthetic Aperture Radar
SF	:	Single Frequency
SNR	:	Signal to Noise Ratio
UWB	:	Ultra wideband

LIST OF VARIABLES

$A_{noiseless}$:	Area under the CPR for AWGN case
A_{noisy}	:	Area under the CPR for ideal case
A_m	:	Target reflectivity coefficients
b_i	:	Coefficients of a given sequence
B	:	Bandwidth
c	:	Speed of light
C	:	Coding scheme
$C_{k,r}$:	Matrix in which its coefficients have conjugate symmetry about columns N and $N + 1$.
C_{pr}	:	Cross range profile reconstruction
d_C	:	Distance between two targets on cross range coordinates
d_R	:	Distance between two targets on range coordinates
D_m	:	Time delaying
\hat{D}_m	:	Delay due to a reference point
f_0	:	Fundamental frequency
$f_0(y)$:	Range domain function
f_{prf}	:	Pulse repetition frequency
F_s	:	Sampling frequency
k	:	Data symbol

L	:	Half range swath
L_a	:	Antenna length
L_{OFDM}	:	Pulse length of the OFDM signal
L_p	:	Pulse length
m	:	Number of target positions
m_s	:	Number of stages
M	:	Number of sequences
n	:	Number of bins samples
n_s	:	Length of a given sequence
N	:	Number of subcarrier coefficients of the OFDM signal
N_{AWGN}	:	Additive white Gaussian noise
N_T	:	Number of targets
$PN(t)$:	PN sequences
R	:	Range distance
R_m	:	Range distance to the target at a given position m
$R(0)$:	Auto correlation value
$R(k, l)$:	Cross correlation between the function k and l
R_{max}	:	Maximum cross correlation value
s	:	Transmit time domain signal
s_{tx}	:	Transmitted signal
$s_t(t)$:	Data signal

\mathbf{S}	:	Transmit frequency domain signal
\mathbf{S}_{rx}	:	Received signal
$s_r(t)$:	Received signal in time domain
$\widehat{\mathbf{S}}_{rx}$:	Received signal with noise
$\mathbf{S}_{transmit}$:	Reference transmitted signal in frequency domain
t	:	Round trip propagation time
$t(m)$:	Cross correlation values
T	:	Time interval between successive pulses
T_s	:	Delay at the starting sampling time
u_c	:	Cross range coordinate at the center of the target
u_m	:	Cross range coordinate of the target at n th time moment
u_0	:	Cross range coordinate at the target position
\widehat{u}_{m0}	:	Estimate of the target location on the cross range axis
U	:	Cross range target coordinates
V_{rm}	:	Radial velocity
V_u^{SAR}	:	Speed of the moving radar (SAR)
Y	:	Range target coordinates
Y_c	:	Range coordinate at the center of the target
Y_0	:	Range coordinate at the target position
\mathbf{Y}_m^R	:	Range profile reconstruction
α	:	Uniform assignment of sub-bands

$\boldsymbol{\beta}$:	Random assignment of sub-bands
β	:	Phase history
β_n	:	Fundamental phase (delay) at the n th point target
ε	:	Error estimate
δx	:	Azimuth (cross range) resolution
$\delta\beta$:	Step interval for the grid search
ΔR	:	Range resolution
δu	:	Sampling step for CPR
\mathcal{F}	:	Fourier transform operator
\mathcal{F}^{-1}	:	Inverse Fourier transform operator
$\theta_{correct}$:	Compensation term for RMC
$\theta(k, r)$:	A vector that defines $\mathbf{C}_{k,r}$
ρ_s	:	Cumulative side lobe level
ϕ_m	:	Phase of a single complex sinusoid
$\boldsymbol{\Phi}_m^{ref}$:	Phase of a single complex sinusoid at the reference signal
τ	:	Pulse duration
$\boldsymbol{\psi}$:	A matrix containing the entry of $\mathbf{C}_{k,r}$ with the transmitted signal S
Γ	:	A matrix describe by $\boldsymbol{\psi}$ entries
w	:	Temporal frequency domain for time t
w_c	:	Center frequency

ABSTRACT

Full Name : Mohammed Dahiru Buhari
Thesis Title : Synthetic Aperture Radar Processing Using UWB OFDM Signals
Major Field : Telecommunication Engineering
Date of Degree : March 2014

This thesis investigates the use of Ultra Wideband (UWB) Orthogonal Frequency Division Multiplexing (OFDM) in Synthetic Aperture Radar (SAR) cross range reconstruction and SAR imaging for single and multiple targets. For the single target, the cross range profile is reconstructed via matched filtering of the estimated phase history with a reference function in time domain, and the performance of the reconstruction process is evaluated in terms of target reconstruction accuracy, the impact of varying the number of subcarriers on the main lobe and side lobe levels of the Cross-range Profile Reconstruction (CPR). It is shown that increasing the number of subcarriers results in an improvement in the target reconstruction but at the cost of having a wider main lobe. For the phase history grid search, it is observed that decreasing the step size will not necessarily give a better result and as such an optimal number of subcarriers depends on the intended scenario.

We later extend the work to multiple targets and present the necessary conditions for the radar to distinguish echoes received from different targets. These conditions are range and cross range resolution. If either of these conditions is satisfied, the receiver can distinguish the different target positions otherwise it will image them as a single large target.

For the SAR imaging, the image is formed by taking the product of each Range Profile Reconstruction (RPR) with the corresponding CPR value. Also Information from the CPR is used for Range Migration Correction (RMC) while OFDM waveforms are designed using uniform/random assignment of the subcarrier vector and Pseudo-Noise (PN) sequences such as Gold and Kasami codes to suppress range ambiguity.

ملخص الرسالة

الاسم الكامل: محمد طاهر بخاري

عنوان الرسالة: معالجة عمليات الرادار ذو الفتحة التركيبية (SAR) باستخدام الترددات المتعامدة فائقة العرض

التخصص: هندسة اتصالات

تاريخ الدرجة العلمية: مارس 2014

هذه الرسالة تدرس استخدام ترميز تقسيم التردد المتعامد (OFDM) ذات النطاق الفائق العرض (UWB) لإعادة تشكيل المسافة العرضية لرادار ذي الفتحة التركيبية (SAR) والتصوير الراداري باستخدام رادار واحد، وذلك لحالتي وجود هدف واحد أو أهداف متعددة. يتم إعادة تشكيل ملف المسافة العرضية عن طريق مرشحات متطابقة مع تاريخ الطور المقدر مع دالة مرجعية في المجال الزمني. ويتم قياس أداء عملية إعادة التشكيل من خلال دقتها في اكتشاف الهدف وأثر التفاوت في عدد الحوامل الجزئية على المنطقة الرئيسية للهوائي، ومستوى المناطق الجانبية للهوائي عند إعادة تشكيل ملف المسافة العرضية. تبين أن زيادة عدد الحوامل الجزئية يؤدي إلى تحسن في دقة إعادة تشكيل الهدف على حساب توسع المنطقة الرئيسية للهوائي. وبالنسبة للبحث الشبكي لتاريخ الطور، لوحظ أن تقليص حجم الخطوة لن يعطي بالضرورة نتيجة أفضل وعلى هذا النحو فإن العدد الأمثل من الحوامل الجزئية يعتمد على السيناريو المقصود. في ما يتعلق بنتائج المحاكاة، باعتبار وجود هدف واحد في المرحلة الأولى، تم مقارنة النتائج مع مرجع الطور لحالة تردد واحد. قمنا بعد ذلك بتوسيع المفهوم نفسه في حالة وجود أهداف متعددة وقدمنا الشروط اللازمة للرادار لتمييز الأصداء الواردة من أهداف مختلفة. عندما تلي الأصداء هذه الشروط، يستطيع المتلقي التمييز بين المواقع المختلفة لهذه الأهداف، وإلا فإنه سيعتبرهم كهدف واحد كبير.

بالنسبة للتصوير الراداري باستخدام رادار ذي الفتحة التركيبية، يتم تشكيل الصورة باستخدام معلومات ملف المسافة وملف المسافة العرضية الذين تم إعادة تشكيلهما. وتستخدم المعلومات من ملف المسافة العرضية المعادة تشكيلها لتصحيح نزوح المسافة (RMC) بينما تصمم موجات ترميز تقسيم التردد المتعامد (OFDM) لازالة الالتباس في المسافات. وتصمم هذه الموجات عن طريق تعيين الحوامل الجزئية بشكل عشوائي منتظم وعن طريق متسلسلات ضووائية مزيفة. النتائج المعروضة تظهر فعالية التقنية المستخدمة لإعادة التشكيل وتصوير الهدف سواء ذلك لهدف واحد أو أكثر.

CHAPTER 1

INTRODUCTION

1.1 Introduction

Radio Detection and Ranging popularly known as RADAR is one of the earliest applications used in military (since World War II) mainly for the purpose of detection and ranging of targets of interest. In the old days, radars were used only in determining range (distance) of targets [1]. However in the late 1960's, radar imaging was introduced and by the mid 1970's it has grown into an important field of research owing to the advancement witnessed in solid state electronics and Digital Signal Processing (DSP) as a result of which the imaging concept is still used today [2]. Although many types of imaging sensors exist (for example optical and Light Detection and Ranging (Lidar) imaging), radar imaging became more popular because of its robustness to many environmental/weather conditions such as rain, lightening and fog. This is due to the fact that radar uses Radio Frequency (RF) signals which has greater level of immunity to such environmental conditions and thus is more reliable, robust and a better option in imaging applications.

In our modern world today, radar finds applications not only in the military but also for civilian purposes such as weather forecast, navigation of ships, police traffic used for enforcing speed limits, air traffic control and non-destructive material test. To use radar for these applications, a high resolution radar image sensor is needed in order to have a clearer

view of the target coordinates. Synthetic Aperture Radar (SAR) offer high resolution images and are mainly used for this purpose. It can be used for both Range Profile Reconstruction (RPR) and Cross range Profile Reconstruction (CPR). For RPR, the signal is processed via matched filtering in fast time whereas in CPR, the signal processing can be done in several ways depending on the SAR signal used. Moreover, cross range imaging largely depends on the SAR system's ability to operate with the phase of the return signal. This is because the CPR (or azimuth) also depends on the phase history of the received signals which in turn requires the analysis of a specific radar signal for the phase history extraction [3].

In general, for a given framework the generic single frequency radar waveform model is seen to derive a spherical shape Phase Modulated (PM) signal form. It is a nonlinear function of target location and the radar position (also known as phase history). High resolution radar imaging can be generated by combining Ultra Wideband (UWB) Orthogonal Frequency Division Multiplexing (OFDM) with SAR [4]. This will make the system resilient to narrow band jamming, noise as well as interference. In particular using UWB OFDM in SAR processing improves the resolution of the reconstructed image which significantly enhance the potential of identifying a target easily. So the objective of this research is to investigate the use of UWB OFDM signals in SAR cross range (axis perpendicular to the range) reconstruction and SAR imaging for single and multiple targets.

1.2 Thesis Organization

After the introduction given in this chapter, the remaining part of this thesis is organized as follows: Chapter 2 gives an overview of the literature from the preliminary study of OFDM SAR to the recent development in the field. Detailed background on the concept of SAR, OFDM and UWB and the benefit of combining these technologies together is also explained. Chapter 3 deals with CPR methodology and simulation of a single target detection of OFDM SAR. This work is extended to multiple target scenes and establishes the necessary conditions to distinguish echoes received from different targets of interest. Chapter 4 describes the idea of Synthetic Aperture Radar (SAR) imaging and the problems associated with range imaging and how to overcome them. Chapter 5 deals with OFDM waveform design for range ambiguity suppression where an investigation is carried out on how to choose the OFDM waveform that can give the best performance. In Chapter 6, we give the summary and conclusions derived from the work as well as future research work.

1.3 Thesis Contributions

A lot of research work has been carried out and is still on going in the field of UWB OFDM SAR. Having gone through the literature, we identify the following research gaps and our contributions focus on these points:

1. For the single target scenario, we look at how to decide on the phase delay given the many received OFDM components. Since the SAR is moving, the phase history will contain many minima and maxima and using grid search with small step size

might not necessarily give the best result. So we look at the effect of the grid search in the choice of the number of subcarriers.

2. Comparing the OFDM SAR with a single frequency, we investigated the tradeoff between increasing the number of subcarriers and the main lobe width of the cross range profile. Points 1 and 2 can then be used to help the designer in a proper choice for the number of subcarriers to use.
3. Most of the previous researchers assumed a single target. Based on this, we extend the work to multiple targets scenes and examined the necessary conditions for the radar to distinguish echoes received from different targets. This is done for both the cross range detection and the SAR imaging process.
4. As there is always a tradeoff between uniform or random assignment of the subcarrier coefficients which results in either low or high range side lobes, we investigated an OFDM waveform design for range ambiguity suppression using PN sequences (such as Gold and Kasami codes) and uniform/random coding.

CHAPTER 2

TECHNICAL BACKGROUND AND LITERATURE

REVIEW

2.1 Introduction

In this chapter, we give a detailed technical background of all the concept involved in OFDM SAR follow by an overview of the literature related to high resolution SAR and OFDM SAR, and OFDM waveform design for range ambiguity suppression.

2.2 Technical Background

This section provides a detail technical background of the concept used in SAR and OFDM. They include the concept of SAR, radar terminologies and functions, basic principles of OFDM, UWB technologies, matched filtering and the benefits of UWB OFDM SAR system.

2.2.1 Concept of Synthetic Aperture Radar

Radar uses modulated waveforms and directive antennas to transmit electromagnet energy into a specific volume in space to search for targets [5]. In other words, radar measure the distance to an object by transmitting electromagnetic wave to the target and receiving an echo of the reflected signal from it. By definition, range is the radial distance between the target position and the radar antenna. Mathematically the range (distance) R is given by

$$R = \frac{1}{2} \times ct \quad (2.1)$$

where t is the round trip propagation time and c is the speed of light.

There are two types of radar, namely Real Aperture Radar (RAR) and Synthetic Aperture Radar (SAR). RARs are radars that are controlled by the physical length of the antenna [4] while SARs are forms of radars whose defining characteristics is the use of relative motion between an antenna and its target region [6]. In other words, a SAR image is produced using a forward movement of the radar. As it passes a given target (scatterer), the signals are reflected, refracted or diffracted. So by recording and combining these signals, a “synthetic aperture” is created which provides an improved imaging resolution. For example, consider the scene in Figure 2.1 in which a SAR moving platform is used to image a target (car). The SAR uses one antenna but in time multiplex. Hence the different geometric positions of the radar is as a result of the moving platform. At each position, the radar records amplitudes and phases of all the returned signals from position A to D . So as the target enters the radar beam, the returned echoes from each transmitted pulse is recorded until the target leaves the view of the radar beam. These recorded echoes are then used in image reconstruction of the target.

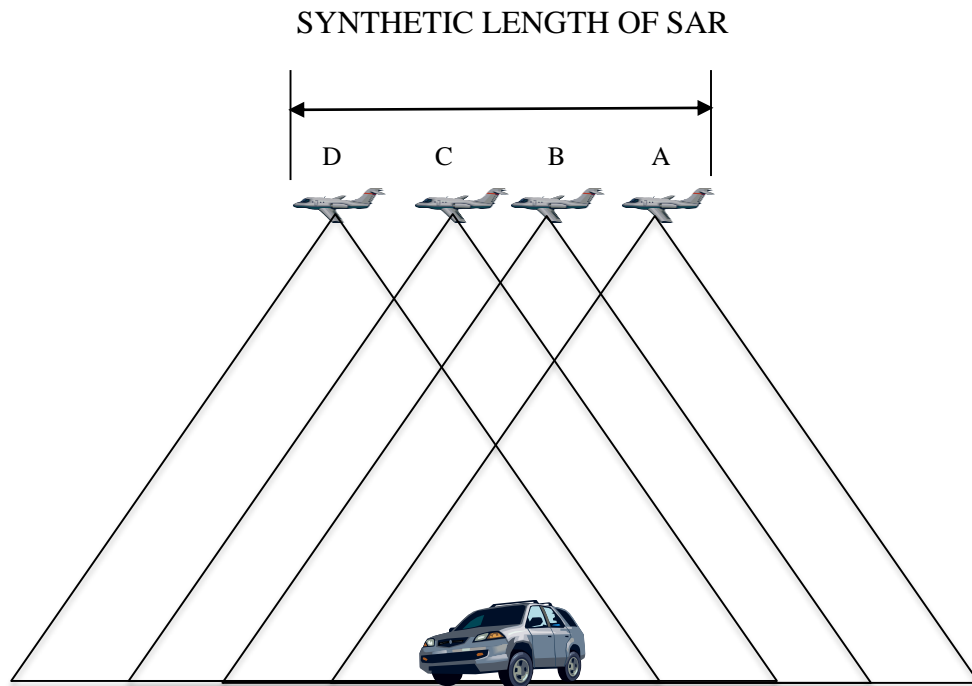


Figure 2.1 Example of an image formation in SAR

2.2.2 Radar Terminology

The understanding of the following parameters is needed in SAR design systems:

Pulse Repetition Interval (PRI) and Pulse Repetition Frequency (PRF)

SAR measurements are taken on a moving vehicle and as such we have to take some parameters into consideration. Given a pulse radar, the transmission and reception process of these train of pulses is as shown in Figure 2.2 [7].

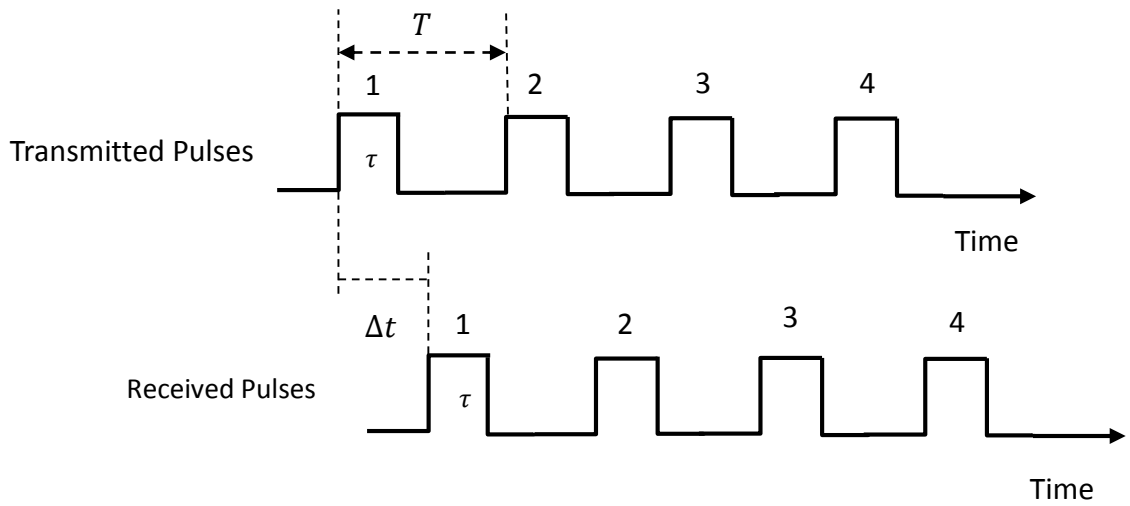


Figure 2.2 PRI and PRF

From Figure 2.2, each pulse has a duration τ and time interval between successive pulses T . This time separation T is called the Pulse Repetition Interval (PRI) and its reciprocal is known as the Pulse Repetition Frequency (PRF). This parameter needs to be controlled for appropriate measurement in SAR.

Range Ambiguity

In any radar system, the range measurement is measured based on the elapses time between the transmission and reception of a signal. To unambiguously measure the range to the target (object), we have to wait sufficiently so that echoes from targets at the maximum range return before the next transmission otherwise ambiguity (uncertainty) will occur in measuring the range. This phenomenon is known as range ambiguity.

The unambiguous range can be obtained by substituting t in equation (2.1) with the PRI T .
i.e.

$$R_{amb} = \frac{1}{2} \times cT \quad (2.2)$$

Equation (2.2) shows that if the target range is less than R_{amb} , the radar can successfully measure its range unambiguously else range ambiguity will occur.

Range Migration

Range migration is a phenomenon that explains the range curvature as the cross range position varies. In other words, the returns from a given target position will be spread over different cross range position as we approach the target. Range Migration Correction (RMC) is employed to cancel this effect. The details of how to perform RMC will become clearer in subsequent chapters. A typical range migration and its correction is as shown in Figure 2.3.

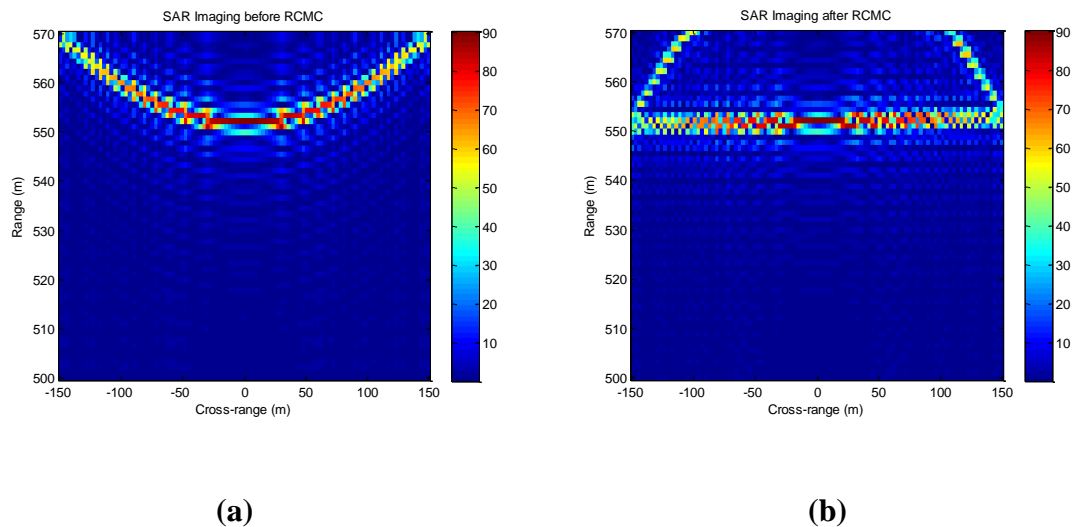


Figure 2.3 SAR imaging (a) Before RMC (b) After RMC

2.2.3 Radar Functions

Most applications of radar can be categorized into detection, tracking and imaging.

Detection means finding the existence of an object of interest within a specific coverage area. This can be done by comparing the amplitude of the received signals with a defined threshold, to decide that a target is present or not.

If we detect the presence of an object, it might be desirable to track its velocity and location. Tracking is beyond the scope of this research and we will concentrate on only detection and imaging.

Radar forms the image of an object by mapping the electromagnetic scattering coefficient index onto a two dimensional plane. Objects with higher coefficient give a higher optical reflective index thereby creating an optical image. Moreover, each pixel (picture element) in a radar image represent a radar reflected echo (backscatter) for that area. Darker areas signify areas with low backscatter while brighter areas represent high backscatter.

2.2.4 Basic Principle of OFDM

OFDM is a multiplexing technique in which a multicarrier system processes signals to be transmitted in parallel at different frequencies simultaneously from the same source. It does so by dividing the available channel bandwidth into many subcarriers that independently send data. The subcarriers are packed tightly together in the frequency domain. Thus, signals from each subcarrier extend into adjacent ones [8]. However as can be seen in Figure 2.4, the frequency response of each subcarrier is designed so that it is zero at the center frequency of the adjacent subcarriers. As such, the subcarriers can therefore be sampled at their center frequencies without interference from their neighbors.

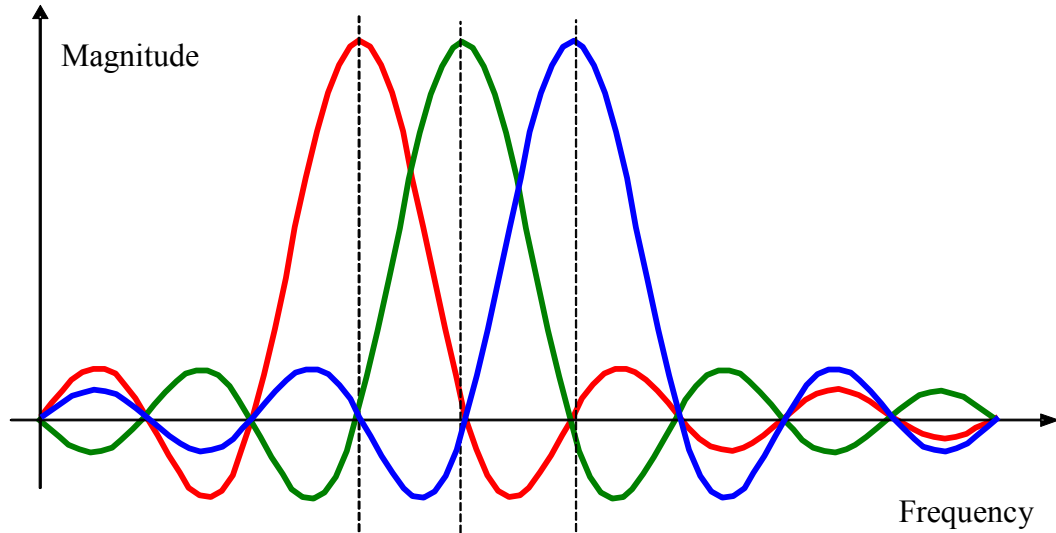


Figure 2.4 OFDM modulation techniques

OFDM finds extensive applications in broadband wired and wireless communication systems mainly because of the way it treat the multipath interference at the receiver. Multipath generates two effects, namely frequency selective fading and Inter Symbol Interference (ISI). The “flatness” perceived by a narrow-band channel overcomes the former while modulating at very low symbol rate eliminates the latter.

In mathematical terms, let $\hat{\mathbf{s}}$ and $\hat{\mathbf{S}}$ represent the double sided vectors of the original OFDM signal with $2N + 1$ samples in time and frequency domain, respectively. Then $\hat{\mathbf{S}}$ can be expressed using

$$\hat{\mathbf{S}} = [0 \ S(1) \ S(2), \dots, S(N) \ S(N) \ S(N - 1), \dots, S(1)] \quad (2.3)$$

where $S(k)$ are real-valued samples of the one-sided vector \mathbf{S} .

The OFDM signal can be represented using

$$S(k) = \sum_{n=1}^{2N+1} \hat{s}(n) e^{-j2\pi \frac{kn}{(2N+1)}}, k = 1, \dots, N \quad (2.4)$$

where N is number of subcarriers and $\hat{s}(n)$ is the k^{th} data symbol of the time domain vector $\hat{\mathbf{S}}$.

However in radar applications, great emphasis is given on the detection of our signal by an enemy and this motivates shortening of the transmitted signal by eliminating the symmetric half of it for transmission purposes. Hence the transmitted signal in time domain (found by taking the Inverse Discrete Fourier Transform (IDFT) of $S(k)$) becomes

$$s(n) = \frac{1}{2N+1} \sum_{k=1}^{2N+1} \hat{S}(k) \cdot e^{j2\pi \frac{(k-1)(n-1)}{2N+1}}, n = 1, \dots, N + 1 \quad (2.5)$$

where $\hat{S}(k)$ are samples of $\hat{\mathbf{S}}$ in frequency domain.

Based on the above definitions, we can deduce that

$$\hat{\mathbf{S}} = [s(2) \ s(3), \dots, s(N + 1) \ s(N + 1) \ s(N), \dots, s(1)] \quad (2.6)$$

2.2.5 UWB Technology

UWB is a promising technology used in transmission of high data rates via low power transmission. It is ideally used for high speed transmission with short range in communication systems. It can be used within a frequency range of 3.1 – 10.6 GHz which gives a bandwidth of more than 7 GHz wide, a transmission rate of 450Mbps, and travel a distance of up to 10 meters. However this bandwidth is regulated by the FCC. The FCC

ruling permits an UWB overlay of the spectrum shown in Figure 2.5 [9]. Also the basic principle of UWB can be explained by the diagram in Figure 2.6.

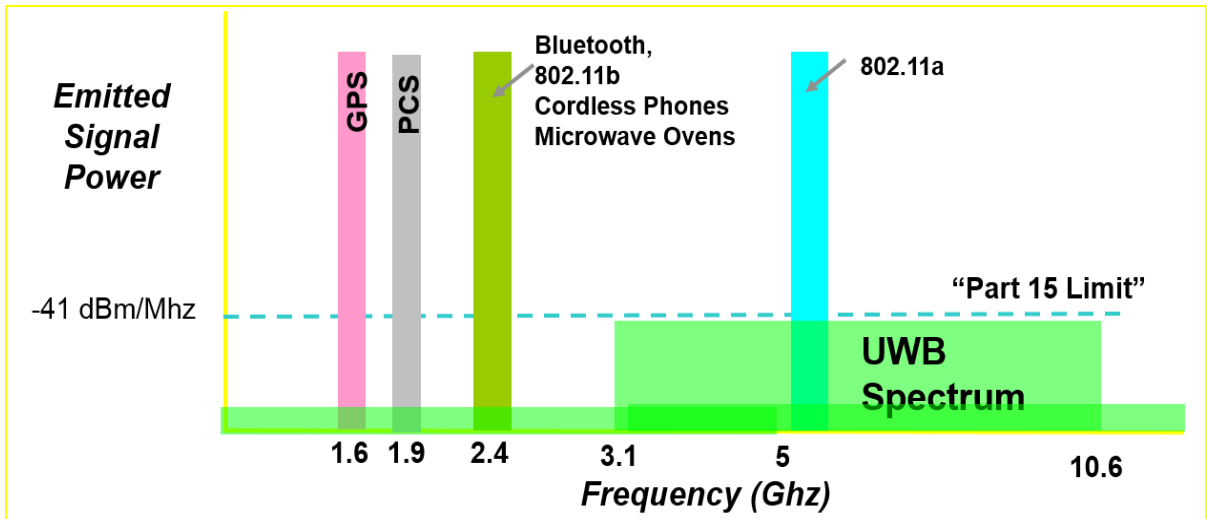


Figure 2.5 FCC ruling for UWB spectrum overlay

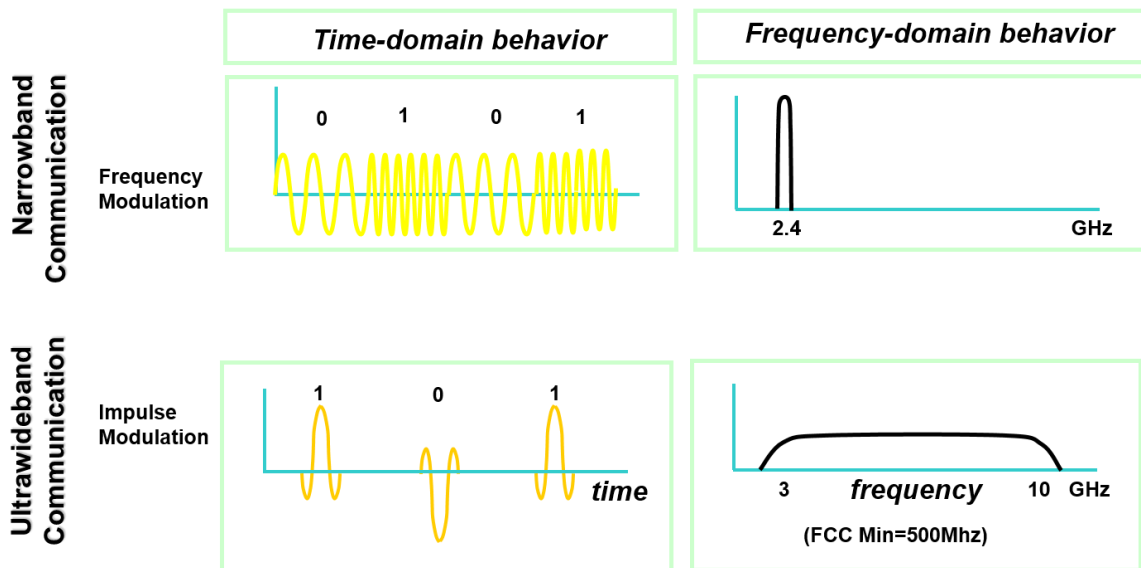


Figure 2.6 UWB behavior in frequency and time domain

Figure 2.6 shows the basic difference between Narrow Band (NB) communications and UWB communications. Most standards for data transmission use NB signals but they operate within a quite narrow frequency band allowing for just small deviations from the carrier frequency. A typical energy distribution of an NB (802.11b) transmitter is shown in the upper right hand corner of Figure 2.6. It has a very narrow spectral band of 20 MHz with a reference frequency of 2.4 GHz.

In contrast to NB, UWB transmits short pulses in time space and distributes all the energy of the pulse within the given wide spectral range (approximately from 3 GHz to 10 GHz). In addition, even though UWB technology generates digital pulses that can be modulated in many ways whether in time, amplitude or phase it can also be modulated directly from the baseband signal as opposed to using a high frequency carrier and as such this renders modulation unnecessary. This in turn gives UWB technology an advantage of having simplicity of design.

In comparison with other technologies, it has the advantage of being faster than Bluetooth and Wi-Fi with data rate of around 450Mbps and can serve as a complementary to IEEE802.11.

2.2.6 Matched Filtering in SAR

Matched filtering is performed by correlating a known signal with an unknown signal in order to extract some relevant information from the received signal that is normally corrupted with noise, interference or both. It is the optimal linear filter for maximizing the SNR [10].

In SAR systems, a matched filter is normally performed by the aid of convolution. Convolution is similar to correlation only with one distinct difference where the signal is time-reversed in the case of convolution. Moreover, we are supposed to get the same signal as the transmitted signal but shifted in time.

In mathematical terms, given a transmitted signal in frequency domain $S_{tx}(\omega)$ and received signal $S_{rx}(\omega)$, the matched filtering operation in time domain is given by

$$s_M(t) = \mathcal{F}^{-1}(S_{rx}(\omega) * S_{tx}(\omega)) \quad (2.7)$$

where \mathcal{F}^{-1} is the Inverse Fourier Transform (IFT) operator.

A block diagram of a typical Matched Filter operation is shown in Figure 2.7.

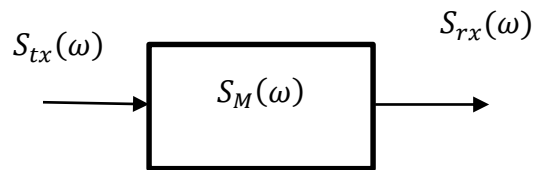


Figure 2.7 Matched Filtering in SAR

2.2.7 Benefits of UWB OFDM SAR System

Combining UWB OFDM, and SAR can bring a lot of advantages to the system (although it will also bring some disadvantages as well). The most notable ones are as follows:

1. High waveform diversity potential: The pulse diversity of OFDM, afforded by ease of signal design is a measure of protection from false target generation.
2. Dual-use architecture (Communications and radar): Combining these technologies give the advantage of using it for dual communication and allows for inexpensive implementation.

3. High resolution and multipath potential: The orthogonality of the OFDM provides the UWB signals with easily processed narrowband components, each of which can be used to improve the accuracy of the system.
4. Ease of narrowband jamming and interference mitigation: Because of the frequency agility and orthogonality of OFDM signals, it is possible to use OFDM SAR in the presence of a jammer, as there is little correlation between the jammer and the radar signal. This makes the system resilient to noise and interference as it will be difficult to read even when it is intercepted. A comparison between OFDM signal with Linear Frequency Modulated (LFM) chirp is illustrated using a spectrogram [11]. Both these signals are generated in baseband and we assumed that the jammer is capable of intercepting it and predicting what was transmitted.

2.3 Literature Review

2.3.1 High Resolution SAR and OFDM SAR

Several research works have been carried out in SAR image processing theoretically and experimentally. One of the earliest and well-studied SAR signal is the Linear Frequency Modulated (LFM) signal. LFM signal permits efficient frequency domain computation methods for Range Doppler Radar processing (a classical approach that continues to receive interest). Among the approaches that are still being explored today is the work of Meta et al [12]. In their approach, Compact-Frequency modulated wave (FM-CW) is combined with high resolution SAR technology which paved a way to many advancement

in radar applications. Peng et al [13] extended the work on FM-CW by integrating a SAR signal into an operational unmanned airborne vehicle.

Other approaches that do not depend on LFM signal include the work of Krieger et al [14] who proposed the use of beam forming using multidimensional signal encoding which enables the generation of SAR systems with flexible imaging capabilities as well as improve the performance of the system. In another development, Gebert et al [15] also gave a practical implementation of the SAR signal with multi-channel azimuth operated in burst mode. However, in all these approaches, a physical implementation of the hardware is needed to be able to get the azimuthal components separately. Amin et al [16] employed a model that uses multipath SAR signals in an urban radar sensing. The model utilizes a propagation through a wall and reflections of interior walls under room surveillance. This permits an implementation of an algorithm that helps in improving the radar system performance effectively. In another related paper [17], a similar approach was used to get a target localization via multipath in order to achieve a localization of a single sensor. The approach used time of arrival (TOA) together with non-linear least squares optimization in order to localize the targets.

With the recent advancement in the use of OFDM in communications, many researchers proposed the use of OFDM in radar applications. The most notable proposal was that of Levanon et al [18] where OFDM signals were used for multicarrier radar applications. As a result interest increased significantly in the use of OFDM signals for radar applications in various research groups (as illustrated in [19], [20] and [21]). An enemy can use specific electronic counter measures to give false imagery information about the target [22],

combining OFDM with SAR will in turn make the model resilient to deception and jamming. Jonathan et al [1] were able to show that because of the frequency agility and orthogonality of OFDM waveforms, it is possible to use OFDM-SAR in the presence of a jammer as there is no correlation between the jammer and the radar signal. Another breakthrough concept in OFDM SAR was introduced by Garmatyuk [23] that is concerned with simulation study of SAR imaging system using OFDM system. He was able to show that OFDM can bring certain benefits such as anti-jamming potential, dynamic spectrum allocation and a possibility of a dual use of communications/Radar.

Yan zhi-guo [24] used multi-resolution feature extraction in target detection of UWB SAR. He looked at the difference between high frequency SAR and low frequency UWB SAR. The method improved the robustness of multi-resolution feature extraction. Chang Yu-lin [25] proposed a method for a moving target focusing and parameter estimation using Range Of Interest (ROI) of multipath channel UWB SAR imaging. Through experimental work, he demonstrated the effectiveness of his method in estimating the target relative velocity, range velocity, azimuth velocity, azimuth position and range position based on ROI. Kauffman et al [26] developed a signal processing method for using OFDM SAR for navigation systems. They [27] developed an algorithm for a novel navigation sensor for UWB OFDM radar. The radar is on board a vehicle that collects data in a strip map SAR configuration flying over an unknown terrain.

Hossain et al [28] used a high resolution potentially jamming-resistant SAR in target reconstruction using Automatic Target Recognition (ATR). The method revealed that UWB OFDM SAR system can be used for anti-jamming purpose through pulse diversity

and can also produce high resolution SAR images. In another development [29], they used an algorithm called Omega- K Algorithm (wKA) to construct SAR images in both friendly and hostile environments. This method enhances the resolution of the image as well as improves the anti-jamming capabilities of the SAR system.

Wein-Qin Wang [30] takes a different approach through the use of MIMO-OFDM SAR for high resolution imaging that later proves to be efficient in spatial diversity gain and improved range resolution. Garmatyuk et al [3] implemented a model for UWB OFDM SAR for image reconstruction using matched filtering in fast time for a 1-D cross range profile reconstruction. Recently, [31] investigated the performance of UWB OFDM SAR cross range in the presence of interference and jamming which also proves resilient to these environmental challenges.

2.3.2 OFDM Waveform Design for Range Ambiguity Suppression

In remote sensing applications, we need a unique signal processor in order to get high resolution of the SAR images. However, a known limitation in SAR system design is range ambiguity phenomenon that occurs as a result of long delayed echoes of the reflected signals. In other words, it occurs as a result of the arrival of unwanted signal after the transmission of a new signal. This is so especially if the current transmitted signal does not contribute in any way to the back scattered signal received after the transmission of the new signal. This kind of echo signal appears as a shadow which can result in a false (ghost) target. To solve this problem, a lot of research has been carried out. A known trade off in SAR range ambiguity is about increasing or decreasing the Pulse Repetition Frequency (PRF) [10]. An increase in PRF result in increasing the azimuth (cross range) ambiguities

while reducing the range ambiguities. On the other hand the reverse is the case if we decrease the PRF. Based on this problem, Vishal et al [32] proposed a technique to increase the PRF without raising the range ambiguity through the use of a coded-OFDM signal and claimed that their approach outperforms conventional chirp signal. In another development [33], OFDM signals were used in SAR system to reduce the cross correlation between each transmitted pulse. Parameters such as Peak Side Lobe Ratio (PLSR), Integrated Side Lobe Ratio (ISLR) and the image resolution were used to assess the image quality and based on the results obtain, the best coded OFDM was chosen. In [34], a similar concept was employed but they added genetic algorithm to optimize the coding of the OFDM signals which improves the different imaging quality parameters. Wen-Qin Wang [35] also proposed a mitigation technique for range ambiguities in high PRF SAR using OFDM wave form diversity. He showed that through the use of OFDM wave form diversity, we can suppressed the range ambiguities as well as offer a large time between products which is suitable for MIMO SAR imaging.

Jabran Akhtar [36] proposed cancellation of the range ambiguities using block coding technique. He used this technique to distinguish echo reflections originating from the recently emitted pulse and those from impending subsequent pulses. To achieve this, he used a simple matched filtering operation at the receiver which permit the use of arbitrary wave forms with potential for waveforms diversity gains. Jian Fang et al [37] used sparse regularization to suppressed the range ambiguity. This can be done using Compressed Sensing (CS) since the recognizable targets are approximately sparse in the ambiguous range zones thus we can reconstruct the main region and also identify ambiguous targets simultaneously. Satyabrata et al [21] proposed an adaptive technique in designing the

spectrum of an OFDM signal in improving the radar range ambiguity using the Wideband Ambiguity Function (WAF). They developed the received signal model incorporating all the scattering coefficients of the target at multiple frequencies. Using this design, they design an optimization algorithm to select the OFDM waveform such that the volume of the corresponding WAF approximates the range ambiguity.

2.4 Research Motivation

Based on the above literature review, UWB OFDM SAR has witnessed a lot of advancement and progress. However based on the literature we reviewed, we find out the following:

- Little work has been done in the use of UWB OFDM in SAR target reconstruction as well as SAR imaging.
- Most of the research conducted in UWB OFDM SAR assumed single target scenario. Therefore expanding the work to multiple target scenario is desirable.
- Because of the range ambiguity in OFDM SAR configuration, coded OFDM is needed. In other words, we need to investigate the choice of the carrier frequency of the OFDM to reduce range ambiguity.

So the aim of this study is to try find solutions to the above mentioned problems.

2.5 Chapter Summary

The chapter provides an overview of the literature in the field of OFDM SAR as well as lays the foundation for a better understanding of what will follow in the subsequent chapters. In the literature review, we started from the first preliminary study on OFDM SAR when it came into light and later looked at the development that follow suit. This gives us a better understanding of what others are doing in this field. In the technical background, we introduced the concept of SAR, OFDM, UWB and the benefits of having them combined together. Some terminologies needed for this research were also explained. In the coming chapter, we will model the scenes for the detection of the targets in cross range and later for downrange detection and imaging.

CHAPTER 3

OFDM SAR CROSS RANGE RECONSTRUCTION

3.1 Introduction

This chapter deals with cross range reconstruction process of a single and multiple targets. The geometric and the signal model are presented and all the parameters needed are explained. Starting with the single target model, we estimate the cross range position of the target and use parameters such as Root Mean Square Error (RMSE), cumulative side lobe levels and the main lobe width to test the accuracy of the estimation process. Also we look at the effect of varying the step interval of the grid search on the number of subcarrier coefficients in target location. For the multiple target scenario, we look at different cases of when the radar can distinguish between one target from another and when not.

3.2 Single Target Cross Range Reconstruction

In this section, the methodology of a single target cross range reconstruction is explained. At first we describe the geometric model, followed by the signal model, phase history estimate and the CPR.

3.2.1 SAR System Geometric Model

Consider a SAR platform shown in Figure 3.1. The radar is mounted on a vehicle moving back and forth within the SAR platform to locate the position of the target by sending

signals towards the target. When the signal reaches the target, part of the signal get refracted, diffracted while other parts are reflected back to the radar as an echo. Due to the nature of the environment, the signal may not reach the radar in a line of sight. The received signal contains information about the location of the target. It is our objective to localize the target position from the received signal.

To develop a system model using SAR geometry, we either use a squint target model in which the center of the target area, (u_c, Y_c) , is not located at the origin of the cross range or we use a broadside target where the center is based at the origin, $(u_c = 0, Y_c)$ as in Figure 3.1. In this thesis, a broadside target model is used. Also for the transmitted/received signal model, we use UWB-OFDM signal because of the advantage of using more OFDM subcarriers. The utilized system model shown in Figure 3.1 follows the work of Garmatyuk et al [26].

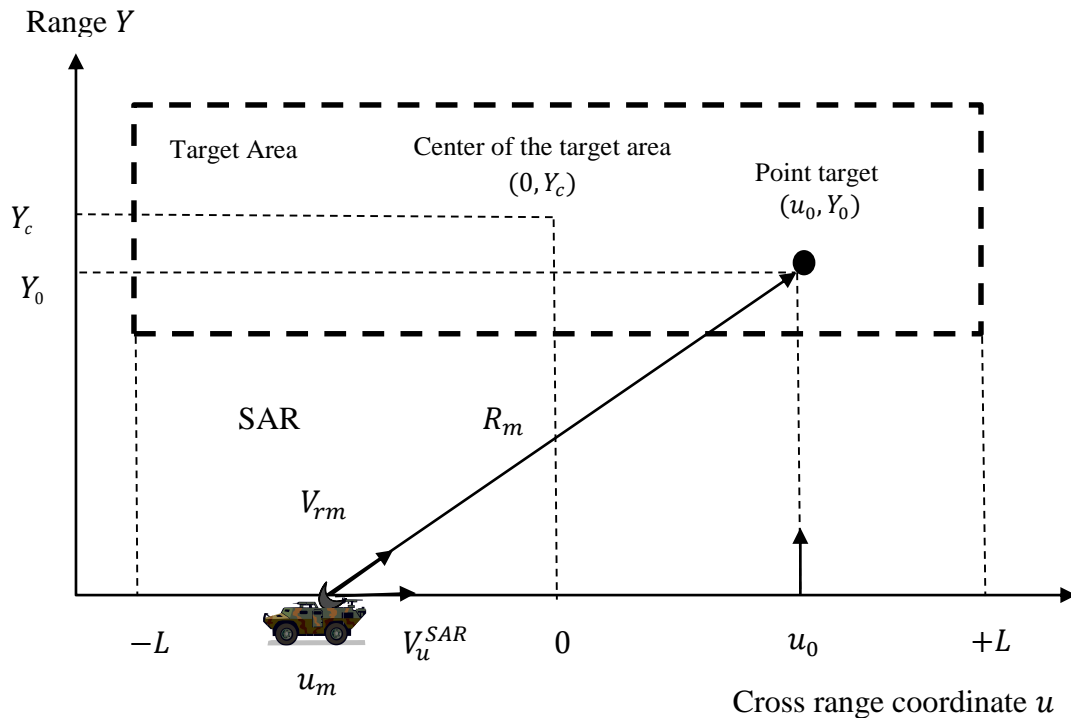


Figure 3.1 Single target system model

The target is located at (u_0, Y_0) and the center of the target is at $(0, Y_c)$. The radar position is located at $(u_m, 0)$ and moves across the SAR platform ranging from $-L$ to $+L$ with a step size Δu . Also the distance between the radar and the target is denoted as R_m and radial velocity measured from the radar to the target is denoted as V_{rm} .

3.2.2 Transmit/Receive Signal Models

For the transmit/receive signal model, a baseband OFDM signal is used. Starting with N number of subcarrier coefficients and using IDFT, a $2N + 1$ samples of the transmitted signal can be generated. The resulting time-domain sampled signal will be truncated to $(N + 1)$ length to remove redundancy. This result is then converted to continuous time-domain using a Digital to Analog (D/A) converter [31]. The continuous transmit signal $s_{tx}(t)$ is given by

$$s_{tx}(t) = \begin{cases} \frac{1}{2N+1} \sum_{k=1}^{2N+1} S(k) \cdot e^{j\frac{2\pi t}{2N+1}(k-1)F_s} & t \in \left(0, \frac{N}{F_s}\right] \\ 0 & \text{Otherwise} \end{cases} \quad (3.1)$$

where $S(k)$ are elements of the frequency domain vector \mathbf{S} ,

$s_{tx}(t)$ is the signal transmitted by the radar as in the model shown in Figure 3.1 to obtain the reflected signal given by

$$s_{rx}(t) = A_m s_{tx}(t - D_m) \quad (3.2)$$

where A_m is the target reflectivity coefficient and D_m is the time delay given by

$$D_m = \frac{2R_m}{c - V_{rm}} \quad (3.3)$$

The reflected signal is sampled with $(N + 1)$ samples to get

$$s_{rx}(n) = \frac{A_m}{2N+1} \sum_{k=1}^{2N+1} S(k) \cdot e^{j \frac{2\pi \left(\frac{n-1}{F_s} (D_m - \tau) \right)}{2N+1} (k-1) F_s}, n = 1, \dots, N + 1 \quad (3.4)$$

where τ is the delay at the starting sampling time.

The true received signal however will be the ideal signal with noise. This noise is added in form of Additive White Gaussian Noise (AWGN).

After generating the transmit/receive signal model, an estimate for the phase history can be formed from the reflected (received) signal.

3.2.3 Phase History Estimate Using Least Square Method

To estimate the phase history, we first convert the received sampled OFDM signals to frequency domain in order to get back the original number of subcarriers N . This can be achieved using DFT. After some mathematical manipulations, the DFT of the received signal is given by [3] [38]

$$S_{rx}(k) = \sum_{n=1}^N s_{rx}(n+1) \cdot e^{-j2\pi \frac{kn}{2N+1}} + \sum_{n=N+1}^{2N+1} s_{rx}(2(N+1) - n) \cdot e^{-j2\pi \frac{kn}{2N+1}}, k = 1, \dots, N \quad (3.5)$$

Equation (3.5) is the DFT of the received signal (Obtained using equation (2.2) and equation (2.3)) which is an expression in terms of the original number of subcarriers in $S(k)$. Also notice that the $e^{-j2\pi \frac{kn}{2N+1}}$ term is $(2N + 1)$ -cyclic. Hence subtracting $(2N + 1)$ from n in the second sum will not necessarily affect its value.

Further simplifications of equation (3.5) leads to [3] [38]

$$\mathbf{S}_{rx} = \frac{A_m}{(2N+1)} \mathbf{\Gamma} \mathbf{\Psi} \quad (3.6)$$

where

$$\mathbf{\Gamma} = \begin{bmatrix} \gamma_{1,1} & \cdots & \gamma_{1,2N} \\ \vdots & \ddots & \vdots \\ \gamma_{N,1} & \cdots & \gamma_{N,2N} \end{bmatrix} \text{ and } \mathbf{\Psi} = \begin{bmatrix} \psi^{1-2N} \\ \vdots \\ \psi^{2N-1} \end{bmatrix}, \quad (3.7)$$

and

$$\psi = e^{-j\frac{\pi\beta}{2N+1}} \quad (3.8)$$

$$\beta = (D_m - \tau)F_s \quad (3.9)$$

$$\gamma_{k,r} = C_{k,r}S(r+1) \quad (3.10)$$

where

$$C_{k,r} = \begin{cases} -\frac{j}{2} [\Theta_1(k,r) + \Theta_2(k,r)], & \text{for } k+r = \text{even}, k \neq r \\ +\frac{j}{2} \left[\frac{1}{\Theta_1(k,r)} + \frac{1}{\Theta_2(k,r)} \right], & \text{for } k+r = \text{odd}, k+r \neq 2N+1 \\ -\frac{j}{2} \Theta_1(k,r) + \frac{2N+1}{2}, & \text{for } k=r \\ +\frac{j}{2} \frac{1}{\Theta_2(k,r)} + \frac{2N+1}{2}, & \text{for } k+r = 2N+1 \end{cases} \quad (3.11)$$

and

$$\begin{aligned} \Theta_1(k,r) &= \tan\left(\frac{\pi}{2} \cdot \frac{k+r}{2N+1}\right) \\ \Theta_2(k,r) &= \tan\left(-\frac{\pi}{2} \cdot \frac{k-r}{2N+1}\right) \end{aligned} \quad (3.12)$$

At the end, the received signal becomes

$$\mathbf{S}_{rx} = \frac{A_m}{2N+1} \mathbf{\Gamma\Psi} \quad (3.13)$$

The next step is to introduce iid AWGN noise into the system to obtain the noisy value of the received signal as

$$\widehat{\mathbf{S}}_{rx} = \mathbf{S}_{rx} + \mathbf{N}_{AWGN} \quad (3.14)$$

where \mathbf{S}_{rx} is defined by (3.13) and \mathbf{N}_{AWGN} is the noise introduced into the system.

Using equation (3.13), we formulate the L^2 -norm to estimate the phase history, β using

$$\varepsilon(\beta) = \|\widehat{\mathbf{S}}_{rx} - A_m \mathbf{\Gamma\Psi}\|^2 \quad (3.15)$$

Through the minimization of this error function, we can obtain an estimate for β . However, equation (3.15) can only be used if we know the value of A_m . But this is not the case in real life as mostly A_m is unknown. As such an estimate for A_m needs to be first derived and then used with equation (3.15) to arrive at the direct expression for the estimate of β (full derivation shown in [3])

$$\hat{\beta} = \operatorname{argmax}_{\beta} \left\| \frac{\widehat{\mathbf{S}}_{rx}^H \mathbf{\Gamma\Psi}}{|\mathbf{\Gamma\Psi}|} \right\|^2 \quad (3.16)$$

Equation (3.16) is the phase history estimate of the received signal which can be used to find the CPR.

3.2.4 Cross Range Profile Reconstruction

Having derived an estimate for β from the OFDM signal, we can now find the phase assuming a single complex sinusoid, which is given by

$$\phi_m = e^{-j2\pi\frac{\hat{\beta}_m}{2N+1}} \quad (3.17)$$

This phase of the single complex sinusoid can be used to find the CPR via matched filtering with a reference function that is given by

$$\phi_m^{ref} = e^{-j2\pi\frac{(\hat{D}_m - \tau)}{2N+1} \cdot F_s} \quad (3.18)$$

where

$$\hat{D}_m = \frac{2\sqrt{u_m^2 + Y_c^2}}{c - V_u^{SAR} \cos(\tan^{-1}(\frac{Y_c}{u_m}))} \quad (3.19)$$

The CPR can be found using

$$\mathbf{C}_{pr}(u_m) = \phi_m^{ref} \otimes \phi_m \quad (3.20)$$

where \otimes is the cross-correlation operator.

Using the CPR of (3.20), we can estimate the actual location of the target by finding the cross range coordinate that makes $\mathbf{C}_{pr}(u_m)$ maximum using

$$\hat{u}_{m_0} = \max_{u_m} (\mathbf{C}_{pr}(u_m)) \quad (3.21)$$

In summary, the methodology for the single target scenario used in this report is as shown in Figure 3.2.

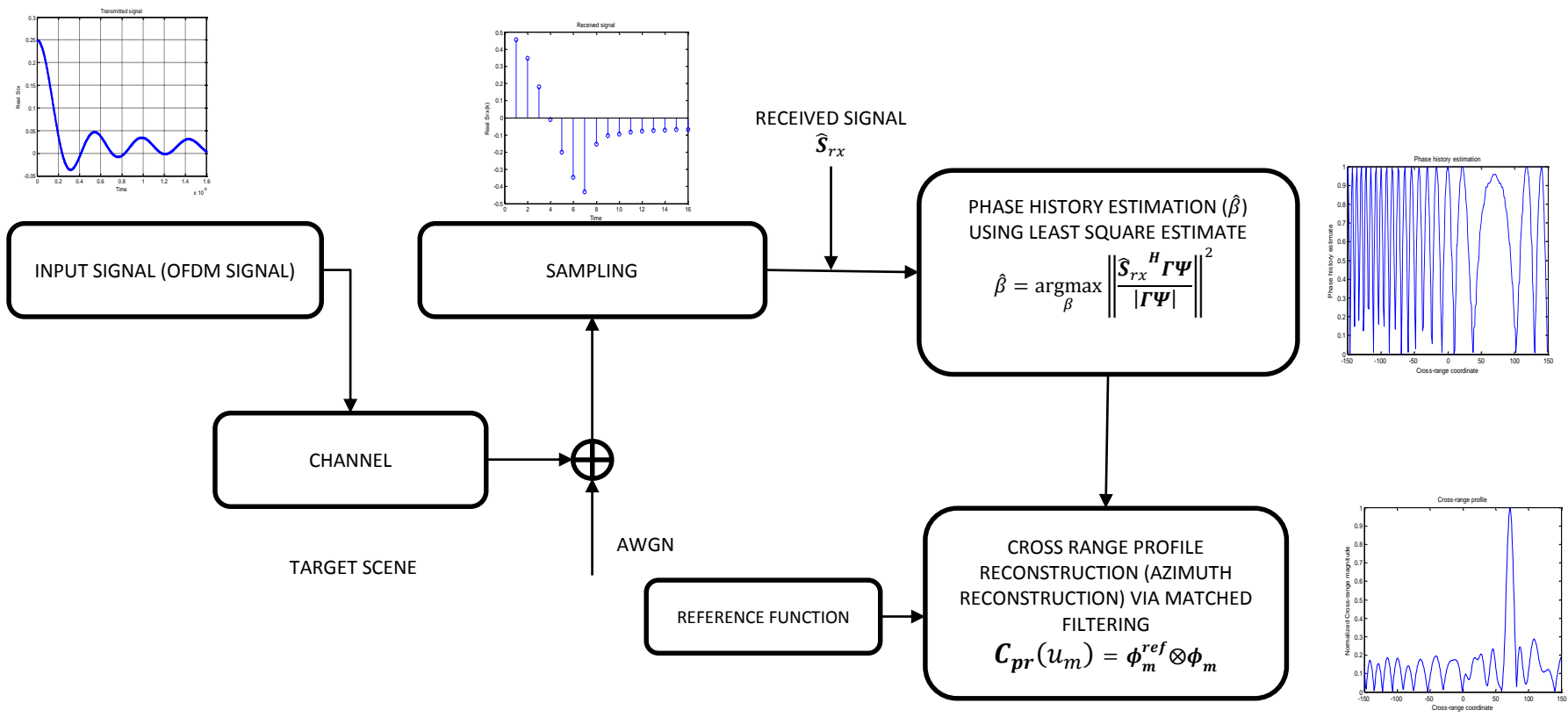


Figure 3.2 Summary of the procedure of a single target cross range reconstruction.

3.2.5 Simulation and Results

In this section, we present the results obtained from the methods described in Section 3.2.2 for the single target scenario. Parameters such as RMSE, cumulative side lobe levels and the main lobe width are used to test the accuracy of the reconstructed CPR. Also we look at the effect of varying the step interval of the grid search on the number of subcarrier coefficients in localizing the target.

To simulate the cross range reconstruction process, we used $N = 4, 8$ and 16 for the number of subcarriers assuming equal energy. The rest of the model parameters are set to the following values (typical of normal conventional SAR): $Y_c = 535\text{m}$; $L = 150\text{m}$; $Y_0 = 520\text{m}$; $u_0 = 70\text{m}$; pulse repetition frequency, $f_{PRF} = 35\text{Hz}$; sampling frequency, $F_s = 1\text{GHz}$, speed of the moving radar, $V_u^{SAR} = 35\text{m/s}$. The number of step size Δu is given by $u=301$. The clutter model used is AWGN through justification by [19].

Using the parameters stated in Section 3.2.2, we evaluate the performance of the reconstruction process using the following parameters:

- i. Root Mean Square Error (RMSE) to quantify the error between the peak location of \hat{u}_{m_0} and the true position of the target u_0 and calculated for all radar positions m . This can be found using

$$RMSE = \sqrt{\text{mean}(\hat{u}_{m_0} - u_0)^2} \quad (3.22)$$

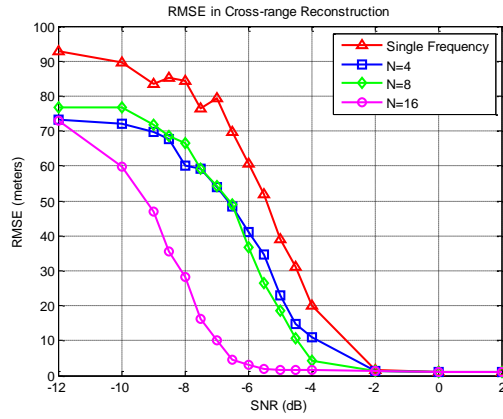
- ii. Cumulative side-lobe level, ρ_s , of the CPR by taking the ratio of the areas beneath the noisy CPR and the noiseless CPR using [38]

$$\rho_s = \frac{A_{noisy}}{A_{noiseless}} \quad (3.23)$$

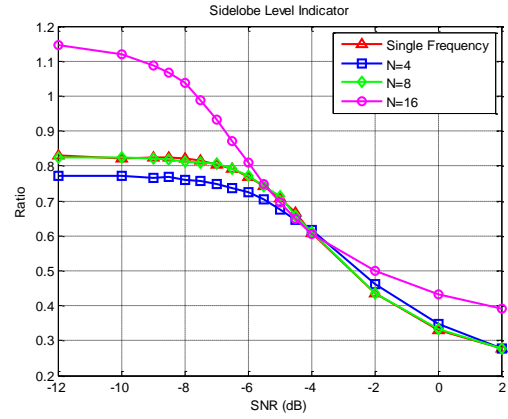
where A_{noisy} is the area under the CPR for the AWGN case and $A_{noiseless}$ is the area under the CPR for the noiseless case.

- iii. Main lobe width, which is a measure of the quality of cross range resolution, is found by taking the 3dB width of the CPR main lobe.

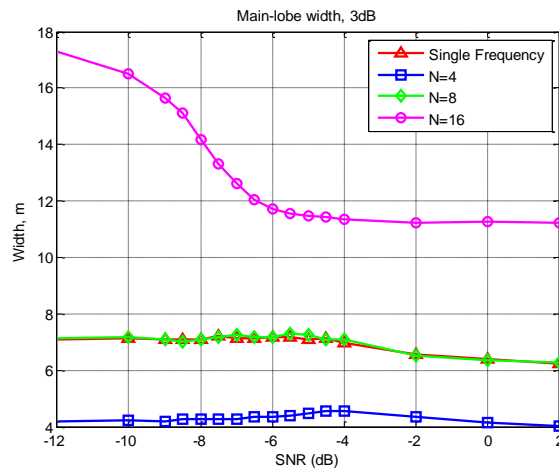
Using these parameters, two cases were considered namely equal subcarrier coefficients and unequal subcarrier coefficients. For the former case, we assume all N sub-bands are ON (ones) while for the latter case, the subcarrier coefficients are generated randomly using uniform distribution. The uniform distribution contains values of zeroes and ones. A 1 means the sub-band is ON while a zero means the sub-band is OFF. Under the same signal to noise ratio conditions, both cases were compared with the Single Frequency (SF) signal evaluated at frequency $f_0 = F_s/17$. This corresponds to the highest fundamental frequency $F_s/(2N + 1)$ of the reference function for the case of $N = 8$. The results obtained are shown in Figure 3.3, and 3.4 respectively.



(a)

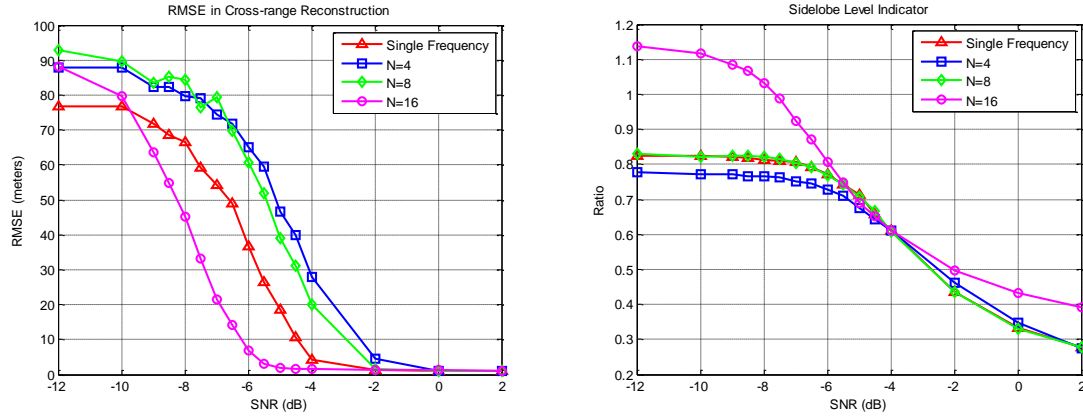


(b)



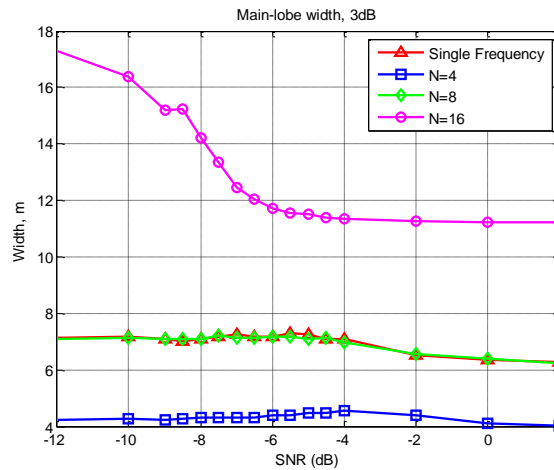
(c)

Figure 3.3 Uniform assignment of the N sub-bands (a) Cross range target position estimation. (b) Cumulative side-lobe level (c) Main lobe width



(a)

(b)



(c)

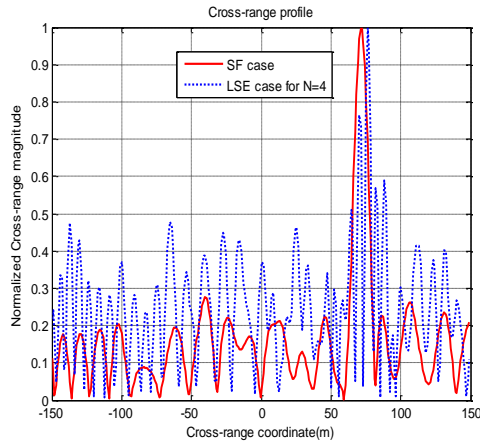
Figure 3.4 Random assignment of the N sub-bands (a) Cross range target position estimation. (b) Cumulative side-lobe level (c) Main lobe width

From Figure 3.3, and 3.4, it can be seen that as the number of subcarriers increases (while keeping the total energy of the signal constant), the RMSE decreases significantly. This is because as N increases, we have more data available for estimation. In comparison to the SF case, we can see that the OFDM case performs better than the SF case for both cases of N for the equal assignment case while for the unequal random assignment, only the case

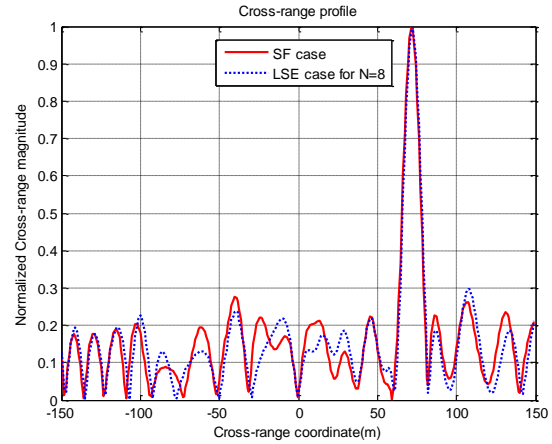
of $N = 16$ performs better than the SF case. This is because equal assignment of N gives the best performance for the OFDM case but is only ideal for friendly environment. In a hostile environment, random assignment of N is desirable in order for the transmitted signal not to be identified even when intercepted. So using higher values of N will be better.

Also in Figure 3.3(a) and Figure 3.4(a), we observed three different regions of interest namely low, medium and high SNR region. In the low SNR region (below $-12dB$) the region is very noisy that choosing a high value of N might even give the worst performance due to the wider main lobe (to be explained), therefore choosing a small N will be a better choice. This first region is not usually the range of interest because the range of error is already very high. In the medium SNR region, $N = 16$ gives a better RMSE compared to either $N = 4$ or $N = 8$. In the high SNR region, all the values of N give the same behaviour and this is expected because as only one carrier is enough for reconstructing the cross range. Therefore choosing a lower value of N will be the better choice.

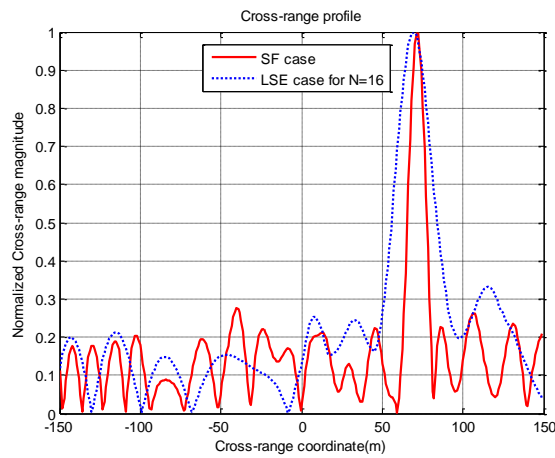
Increasing the number of N results in widening the main lobe as shown in Figure 3.3(b). This is true because looking at the fundamental frequency $F_s/(2N + 1)$, as N increases, the fundamental frequency decreases and hence the main lobe tends to become wider and wider. This is why $N = 8$ gives a better result than the case of $N = 16$. So to use a higher value of N , we have to pay the price of having a wider main lobe. To see this phenomenon clearly, we investigate this effect in details for the Least Square Estimation (LSE) of the CPR using different values of N ($N = 4, 8, \text{ and } 16$) and compare the performance with the SF signal at SNR of $1dB$. The results are shown in Figure 3.5. This affects the number of needed measurements in the cross range, u .



(a)



(b)



(c)

Figure 3.5 Normalized Cross range profile for (a) $N = 4$. (b) $N = 8$. (c) $N = 16$

It can be seen from Figure 3.5 that as N increases, the model behaves more like the SF case but the main lobe becomes wider and wider as observed earlier on SNR plots. This shows that the value of N must be traded off to achieve a better performance.

Effect of Varying the Grid Search on N

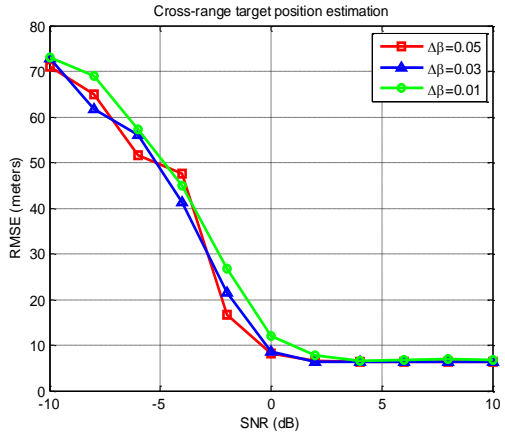
Grid search method is used when we have a multiple dimensional variable for an optimization problem. Moreover as the spectra of the grid search has a complex structure comprising of many minima and maxima residual, there is need to find the global minimum. Using grid search method, we can easily find the global minimum if it is very close to zero and located in a narrow region which distinguishes it from other local minima. For a SAR system, because of the fact that the radar is constantly changing positions the phase history β contains many minima and maxima and therefore care must be taken in choosing the right step interval $\Delta\beta$ for the grid search. This can be controlled by the sampling step, Δu , for the CPR . It has been shown that the sampling step of the CPR is given by [3]

$$\Delta u \leq \frac{c(2N+1)\sqrt{Y_0^2+4L^2}}{8L.F_s} \quad (3.24)$$

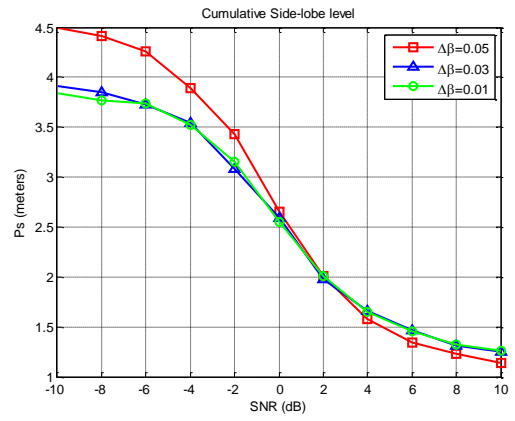
where Δu is the sampling step and the rest of the parameters have their normal definitions.

So since Y_0 , L , c and F_s are fixed in our analysis, by varying the number of subcarriers N , we can observe the effect of the grid search on the estimate we are making. Using $N=4$, 8, and 16, we find the RMSE and the cumulative side-lobe level for different values of the step size $\Delta\beta = 0.05$ (step size $u = 301$), 0.03 ($u = 601$) and 0.01 ($u = 1201$).

The results are as shown in Figure 3.6, Figure 3.7, and Figure 3.8, respectively.

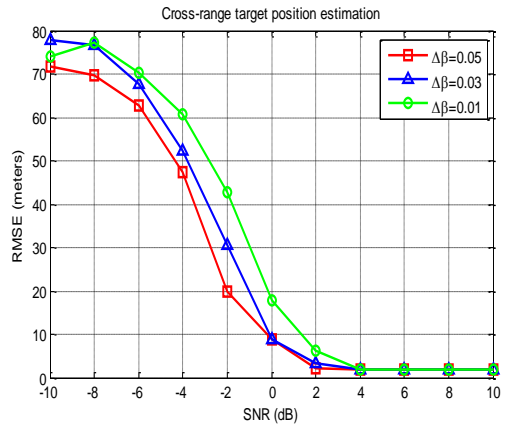


(a)

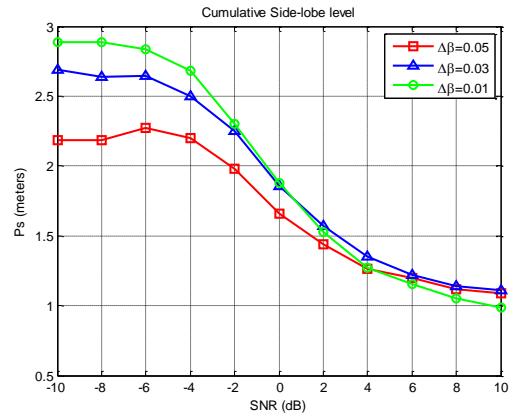


(b)

Figure 3.6 Grid search for $N=4$. (a) Cross range target position estimation (b) Cumulative side-lobe level.



(a)



(b)

Figure 3.7 Grid search for $N=8$. (a) Cross range target position estimation. (b) Cumulative side-lobe level.

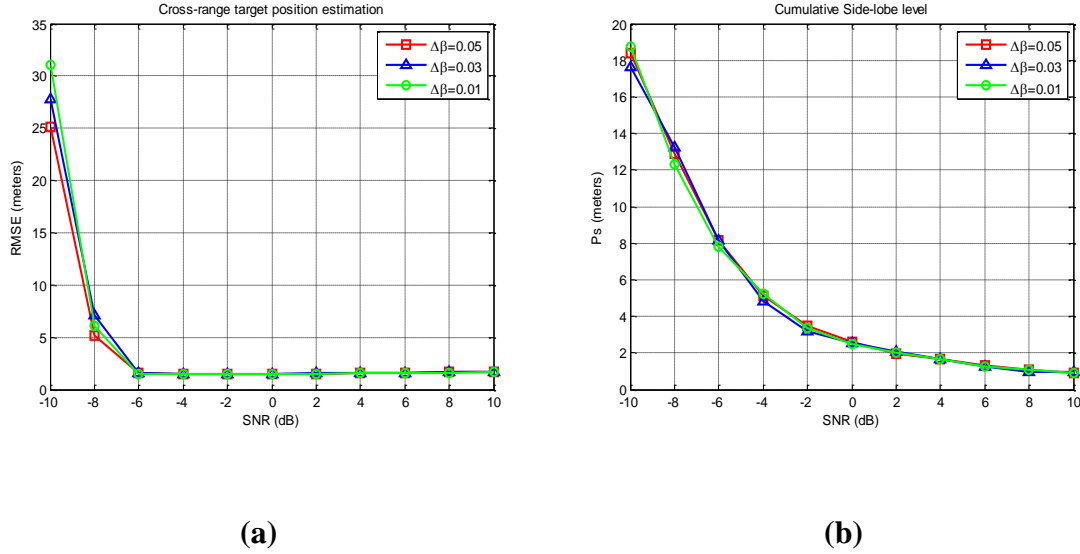


Figure 3.8 Grid search for $N=16$. (a) Cross range target position estimation. (b) Cumulative side-lobe level.

From Figure 3.6, 3.7, and 3.8, we can see that for different values of N and for the specific target position, the grid search behaves in a different way. Whereas the performance of the system improves by decreasing the step interval $\Delta\beta$ for the case of $N=4$, the reverse is the case for $N=8$ and almost has no effect when $N=16$. This also shows that as N increases, variations in $\Delta\beta$ becomes insignificant and the system behaviour improves. This is because as N increases, we have more carrier with different wavelength and hence more phase resolution for estimation.

3.3 Multiple Targets Cross Range Reconstruction

In this section, we describe the reconstruction process of a multiple target model. The procedure for estimation is similar to the single target model only that more targets are now present in the scene. After we establish the system geometry, the same signal model and

methodology of the single target scenario are employed here and in the course of this discussion, we will see how they differ. Reconstruction process of multiple targets is possible if we meet some certain conditions.

3.3.1 Multiple Targets SAR Geometry

When we have more than one target, additional requirements come into play for the radar to distinguish between two or more closely spaced targets (objects). Echoes from the targets must be received at different times for the radar to properly distinguish them. To understand these requirements, we first consider the case of two targets and later extend it to more than two targets. The system model is as shown in Figure 3.9. These requirements are as follows:

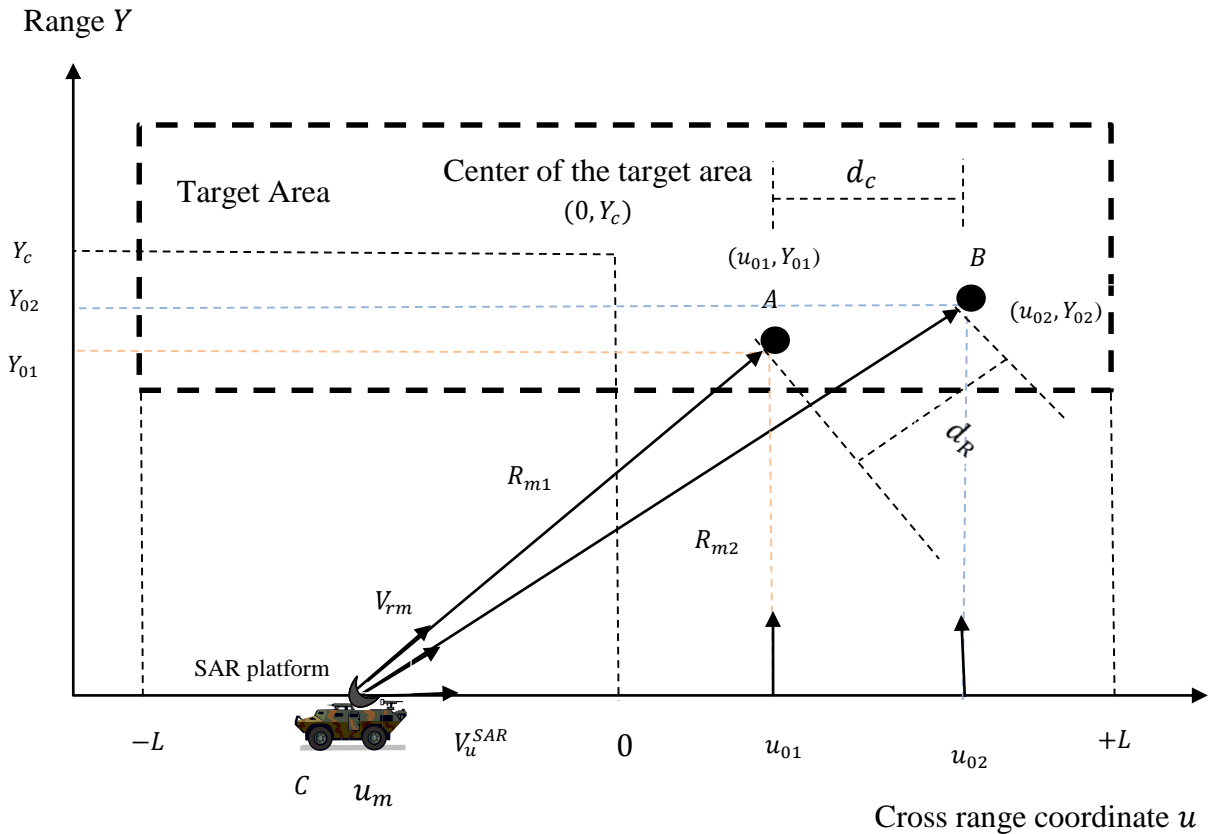


Figure 3.9 System model for two targets scenario

3.3.2 Range Resolution

Consider the geometric model shown in Figure 3.9 which follows the same model for the single target scenario only that the number of the targets is now two. Assume a pulse of length L_p is approaching the two targets and the slant range distance between the two targets is d_R and cross range spacing d_C . The part of the signal reflected by object A is AC while that reflected by B is BC . To reach the target and come back, BC has to cover an extra distance of $2d_R$ and thus is at slightly shorter distance than L_p behind AC . Because of this, the end of AC and the beginning of BC overlap when they reach the receiver. As a consequence, they are imaged as one single large target which extends from A to B . The question that normally arise is when can the radar distinguish echoes from the different targets? This can be answered by the necessary condition that $d_R > L_p/2$. So once the slant range distance d_R between A and B is slightly greater than $L_p/2$, the two-pulses would not overlap and the radar can distinguish between the two-echoed signals from the targets in terms of the range coordinates. The distance d_R is known as the range resolution denoted as ΔR . For a pulse radar, the range resolution can be found using

$$\Delta R = \frac{cL_p}{2} = \frac{c}{2B} \quad (3.25)$$

where B is the bandwidth.

From equation (3.25), we can see that the range resolution improves as we increase the bandwidth. In other words, systems with higher bandwidth have better range resolution. Figure 3.9 shows the variation of range resolution with bandwidth. We can see that a resolution of 1.5 m will be achieved with a bandwidth of 100MHz theoretically. However,

this chapter deals with cross range reconstruction of the target and the range resolution will not play a role here. We will revisit the range resolution condition in chapter 4.

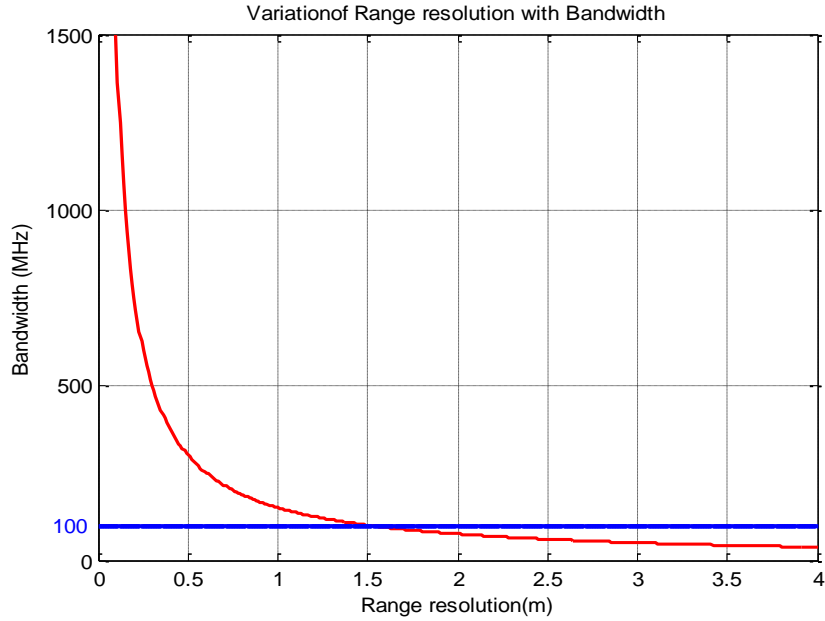


Figure 3.10 Variation of range resolution with bandwidth

3.3.3 Cross Range Resolution

Cross range (azimuth) resolution describes the ability of an imaging radar to separate two closely spaced objects in the direction parallel to the motion vector of the sensor and it is a function of the antenna beam width. It has been shown that the azimuth resolution, δx , of a SAR system with an antenna of aperture size L_a is given by [10]

$$\delta x = \frac{L_a}{2} \tag{3.28}$$

The azimuth resolution is half of the size of the antenna aperture. One of the greatest advantage of SAR system is that they achieve very good azimuth resolution which is independent of the slant range and this is a desirable result for imaging. From Figure 3.9, if the cross range spacing d_c between the targets is less than, δx , the radar will image them as one single large target. On the other hand, if $d_c > \delta x$, the radar can resolve the targets. The cross range resolution is responsible for the cross range reconstruction of the target. Once the cross range resolution condition is met, the radar can distinguish between echoes from different target otherwise it will image the targets as one.

3.3.4 Simulation and Results

Using the requirements stated in Section 3.3.3 (cross range resolution), we can reconstruct multiple targets scenes using the single target model previously obtained. The result at the receiver will then be a superposition of the individual received signals from the individual targets. The spherical phase function can be reconstructed using [26]

$$\phi_m^{N_T} = \sum_{n=1}^{N_T} e^{-j2\pi\frac{\beta_n}{2N+1}} \quad (3.29)$$

where β_n is the fundamental phase (delay) at the n^{th} point like target and N_T is the number of targets.

As a rule of thumb, the number of subcarriers N of an OFDM SAR signal must be greater than the number of the targets N_T i.e. $N > N_T$ [26].

Moreover since we are dealing with cross range reconstruction in this chapter, a fixed range position $Y_0 = 520m$ is used for all the targets and the following cases are considered:

Case I : Closely Spaced Targets ($d_C < \delta x$) :

Closely spaced targets means the targets are closely spaced to each other on the cross range coordinates and the spacing, d_C is less than the cross range resolution, δx . For the two targets scenario, we use $u_{01} = 70m$, $u_{02} = 80m$ and $N= 16$ in the simulation and the result is shown in Figure 3.11.

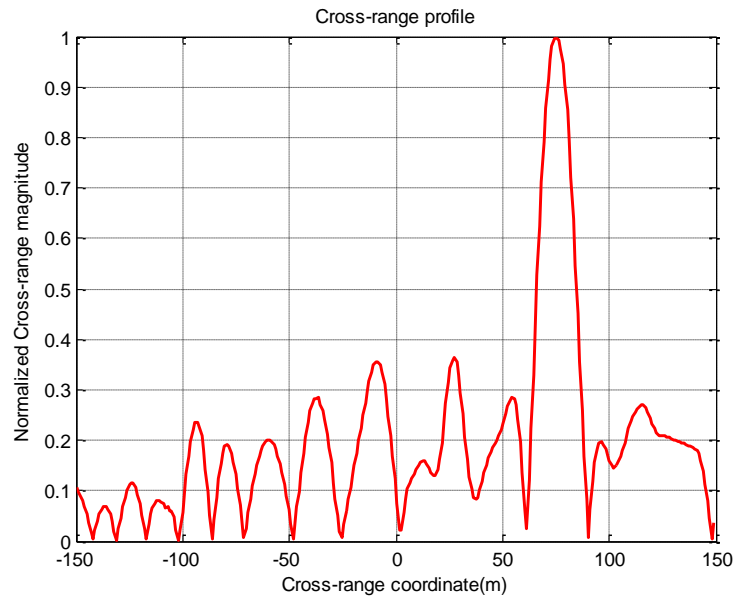


Figure 3.11 Cross range profile for the case of two targets when $d_C < \delta x$

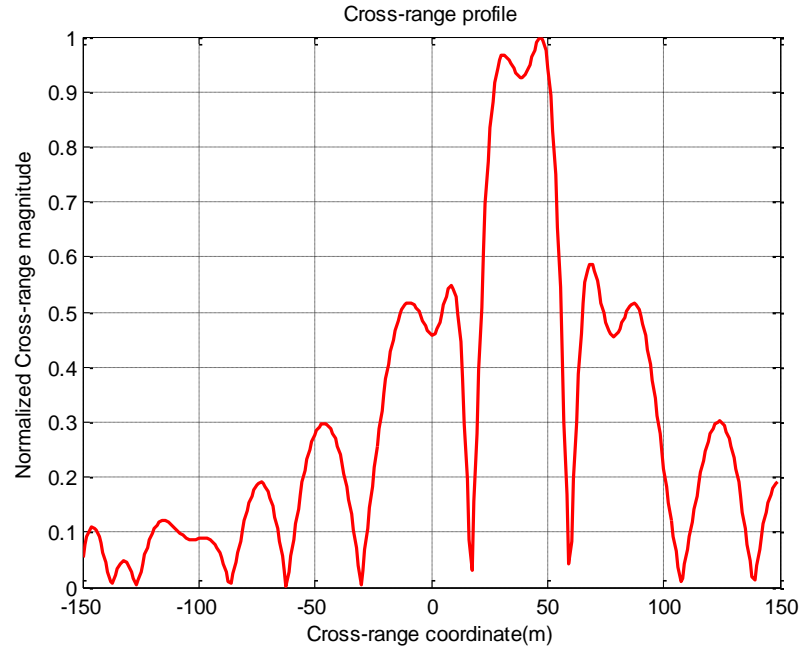


Figure 3. 12 Cross range profile for the case of multiple targets when $d_c < \delta x$

From Figure 3.11, we can see that because the targets are close to each other (i.e $d_c < \delta x$), the radar imaged the two targets as one single large target extending from 70 to 80m. In the same vein, if we consider more than two targets closely spaced to each other, the radar will still image them as one single large target extending from the first target to the last. For illustration, we simulated the CPR for 15 equally weighted equidistance point like distributed cross range from 20 to 55m and the result is as shown in Figure 3.12.

Case II: Separated Targets ($d_c \geq \delta x$) :

Separated targets means that the two targets are far away from each other satisfying the condition $d_c \geq \delta x$. For the two targets scenario, we demonstrate this by using $u_{01} = 40m$ and $u_{02} = 90m$ in the simulation and the result is as shown in Figure 3.13.

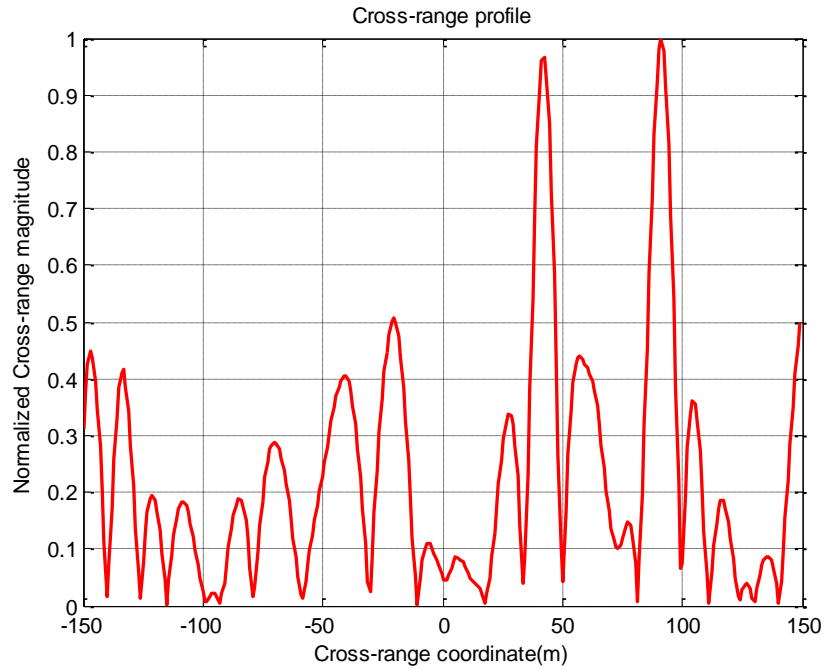


Figure 3.13 Cross range profile for the case of two targets when $d_c \geq \delta x$

From Figure 3.13, we can see that in this scenario, the radar successfully distinguish between the two targets positions. For the case of more than two targets, we simulated the CPR of 4 equally weighted equidistance point like distributed cross range position at -130, -45, 45 and 130m respectively and the result is shown in Figure 3.14.

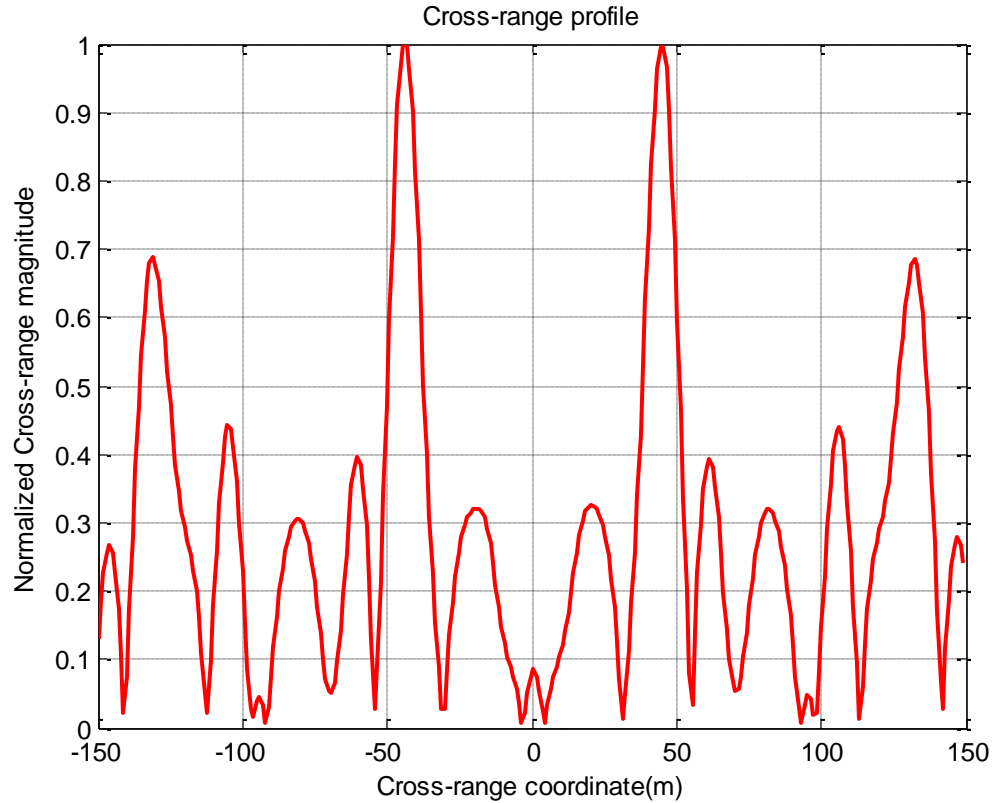


Figure 3.14 Cross range profile for the case of multiple targets when $d_c \geq \delta x$

From Figure 3.14, we can see that even with the presence of multiple targets, the radar still successfully distinguish the position of each targets. However it is important to note that as we have many targets present, the probability of making error in the position of the target increases. This probability of error is known as probability of false alarm and it can be taken care of by setting a threshold level of which each response of the target has to reach before it can be recorded as target positions otherwise it will be discarded.

3.4 Chapter Summary

This chapter deals with the detection process of single target and multiple targets scenarios. For the single target scenario, the geometric and signal model was presented and using the received signal of this model, we estimated the phase history which was later used in cross range profile reconstruction via matched filtering. In the simulation results, parameters such as RMSE, main lobe width and cumulative side lobe level were used to examine the accuracy of this approach. It was observed that as we increase the number of subcarriers, the performance of the system improves, however the main lobe become wider. We also observed that for different number of subcarriers, the grid search for the phase history behaves in a different way. Whereas the performance of the system –for the specific considered parameters- improves by decreasing the step interval $\Delta\beta$ for the case of $N = 4$, the reverse is the case for $N = 8$ and almost has no effect when $N = 16$. This is true because as N increases, we have more data available for estimation.

For the multiple targets scenario, we looked at the case of having multiple targets within the region of interest. At first, we discussed the necessary conditions needed for the radar to distinguish between the echoed received from different targets. One of the condition is that the cross range spacing, d_C , must be greater than the cross range resolution $\delta\chi$. However we see that as the number of targets increases, the probability of detecting a false target also increases. This can be taken care of by setting a threshold for the amplitude of the CPR.

CHAPTER 4

SAR IMAGE RECONSTRUCTION

4.1 Introduction

Since its inception radar has been used primarily for detection and tracking, however with advancement in technology, it is now used for imaging of 2D and 3D scenes. SAR imaging is normally used for 2D imaging and often applied for imaging of static ground scene. In particular, SAR imaging is used when general information of a broad target is needed like in surveillance and reconnaissance [10]. To develop a SAR image, two pieces of information are needed namely range imaging and cross range imaging. In subsequent sections, we will discuss how to form the image for the UWB-OFDM radar.

4.2 Range Imaging

In SAR imaging, the range is the distance of the target that is perpendicular to the motion of the SAR platform. A 2D range imaging system is shown in Figure 4.1.

From Figure 4.1, given a fixed cross range, each of the targets that are within the coverage area of the antenna will have a range Y_n and a reflectivity A_n . For N_T number of targets, the range domain function $f_0(y)$ is given by

$$f_0(y) = \sum_{n=1}^{N_T} A_n \delta(y - y_n) \quad (4.1)$$

where y_n is the range position of the target at position n and $\delta(\cdot)$ is an impulse function.

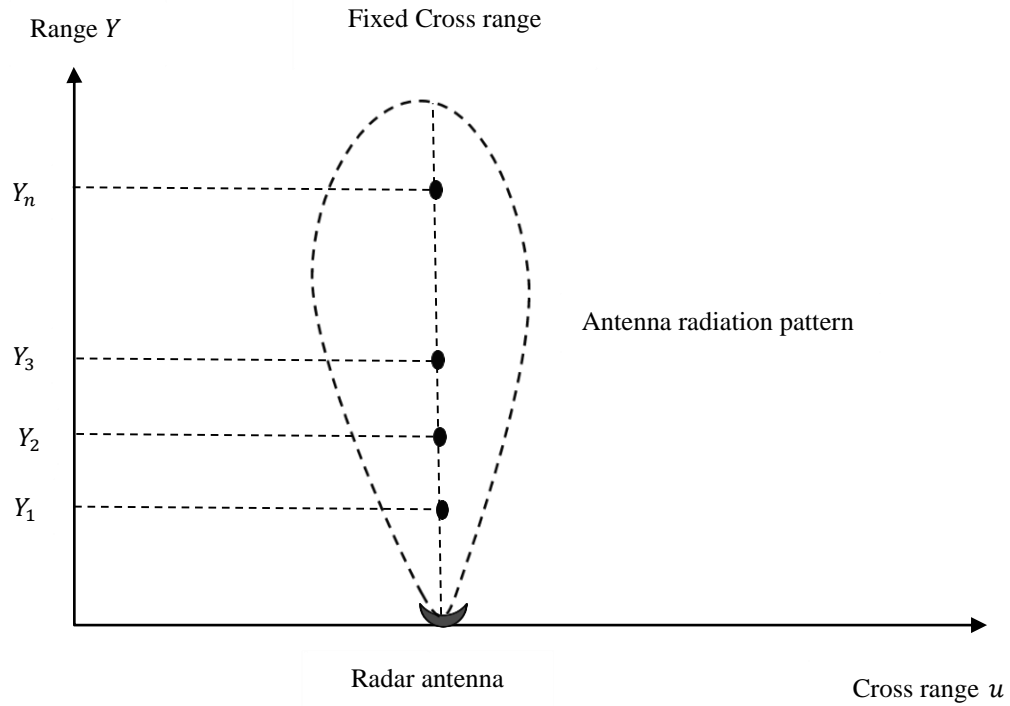


Figure 4.1 SAR Range Imaging

From the model we developed in Chapter 3, the range profile reconstruction at a given cross range u_m is given by

$$\mathbf{Y}_m^R(t) = \left| \mathcal{F}^{-1} \left(\mathbf{S}_{transmit} \cdot (\widehat{\mathbf{S}}_{rx}) \right) \right| \quad (4.2)$$

where $\mathbf{Y}_m^R(t)$ is the range profile (range imaging) in time domain at a given cross range position m and the superscript R indicates range, \mathcal{F}^{-1} is the Inverse Discrete Fourier Transform (IDFT), $\mathbf{S}_{transmit}$ is the reference transmitted signal in frequency domain and $\widehat{\mathbf{S}}_{rx}$ is the received signal corrupted with noise. $\mathbf{Y}_m^R(t)$ is converted from the time domain

to the range domain $Y_m^R(y)$ using $t = \frac{2y}{c}$. So using the parameters presented in Chapter 3, we simulate the range imaging $Y_m^R(y)$ and the result is shown in Figure 4.2. The target is placed at position $(u_0, y_0) = (0, 530m)$.

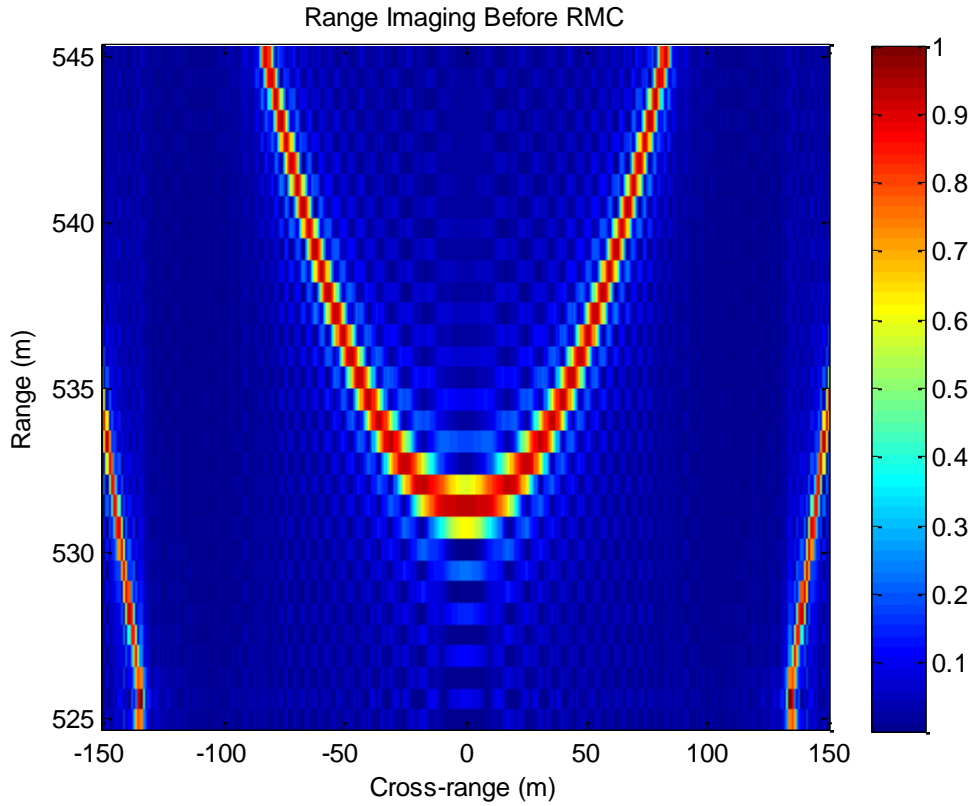


Figure 4.2 SAR Imaging before RMC

From Figure 4.2, it is clearly seen that range migration has occurred. This is because the range is a function of the radar position and the relative velocity between the radar and the target. As a result, the image obtained is distorted and that is what is responsible for the hyperbolic shape in the range imaging. To solve this problem, we need the cross range information.

4.3 Range Migration Correction (RMC)

In SAR, since the radar moves along the cross range coordinates during the data collection process, the cross range information can be used to reduce the problem associated with range migration.

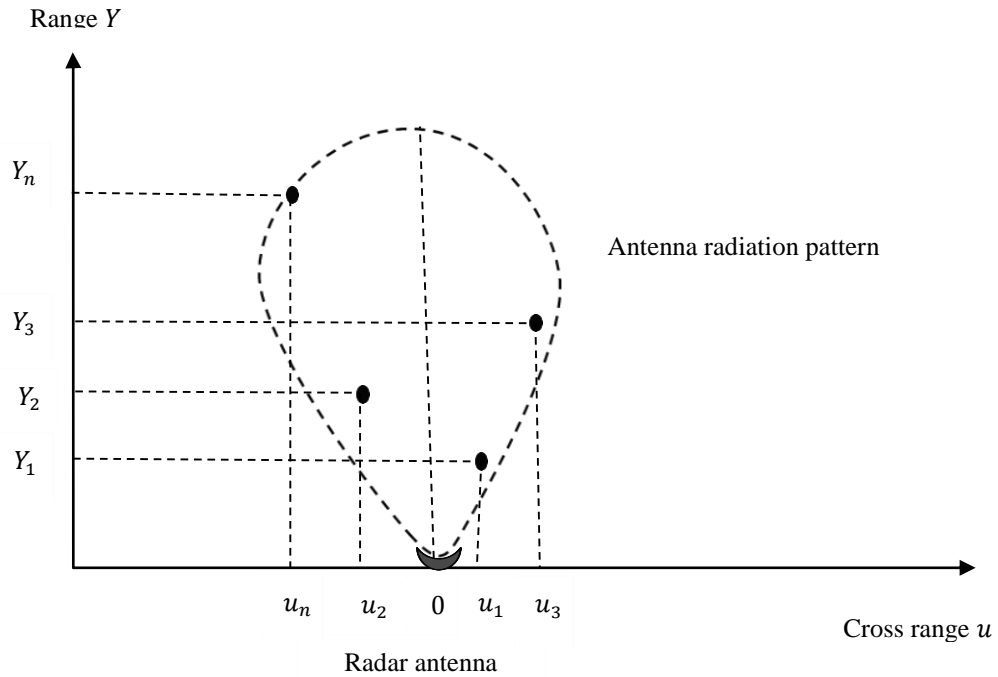


Figure 4.3 SAR Cross range Imaging

Looking at the cross range illustrated in Figure 4.3, we can see that each target that is within the coverage area has a cross range u_n and reflectivity A_n . Also given N_T targets, the received signal is given by

$$S_r(t, u) = \sum_{n=1}^{N_T} A_n S_t(t - t_n) \quad (4.3)$$

To improve the image in Figure 4.2, we need to correct the migration in range through a process known as Range Migration Correction (RMC). This can be done as follows:

From equation (3.20) in Chapter 3, we established the matched filter equation for the CPR. Using this equation, we find an estimate of the actual target position in cross range as shown by equation (3.21). These two equations are used to compute the phase correction term for the RMC.

Expanding equation (3.3) using geometry

$$D_m = \frac{2\sqrt{y_0^2 + (u_0 - u_m)^2}}{c - V_{rm}} = \frac{2y_0}{c - V_{rm}} + \frac{(u_0 - u_m)^2}{y_0(c - V_{rm})} \quad (4.4)$$

The second term in equation (4.4) is what is responsible for the curvature obtained with the range. This can be taken care of by introducing a compensation term $\theta_{correct}$ at each cross range position u_m given by

$$\theta_{correct}(u_m) = \frac{(u_0 - u_m)^2}{Y_c(c + V_u^{SAR} \cos\left(\arcsin\left(\frac{Y_c}{\sqrt{y_0^2 + u_m^2}}\right)\right))} \quad (4.5)$$

Using this correction term, we now update our received signals to become

$$\widehat{\mathbf{S}}_{rx_{new}} = \widehat{\mathbf{S}}_{rx} \cdot e^{j\omega\theta_{correct}(u_m)} \quad (4.6)$$

So if we use $\widehat{\mathbf{S}}_{rx_{new}}$ in place of $\widehat{\mathbf{S}}_{rx}$ in equation (4.2), we can solve the problem of the curvature shape associated with the range imaging. We employed this correction process and the result is as shown in Figure 4.4.

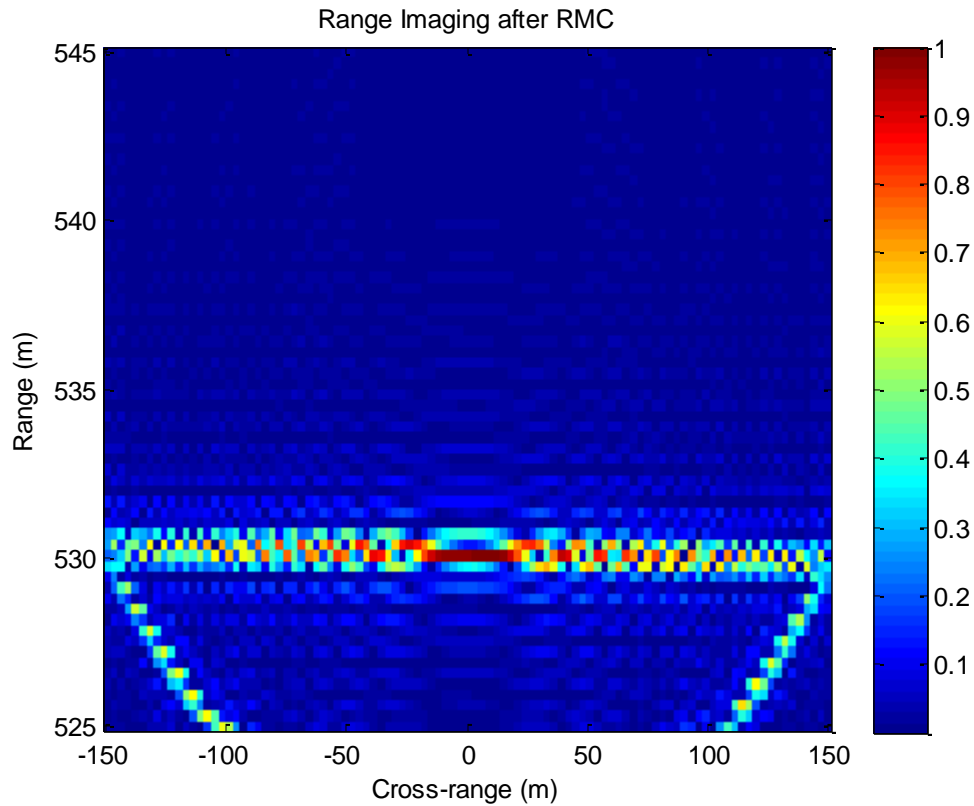


Figure 4.4 SAR Imaging after RMC

From Figure 4.4, we can see that the problem of the curvature shape associated with the range has been eliminated and we now have a straight line. However, we still have the problem of range ambiguity which will be discussed later.

4.4 SAR Imaging

After forming the range and the cross range profiles, we can now use them to obtain a reconstructed image of the target area. At each radar location u , an OFDM signal is transmitted, received and matched filtered. Also the range profile obtained at this position is stored so that in the end, a matrix containing range profiles for each of the radar positions

is formed. The rows of the matrix contain the range profiles while the columns contain the range. To form the 2D-SAR image, we simply take the product of each range profile with the corresponding CPR value. The summary of the procedure of forming the 2D SAR image is shown in Figure 4.5.

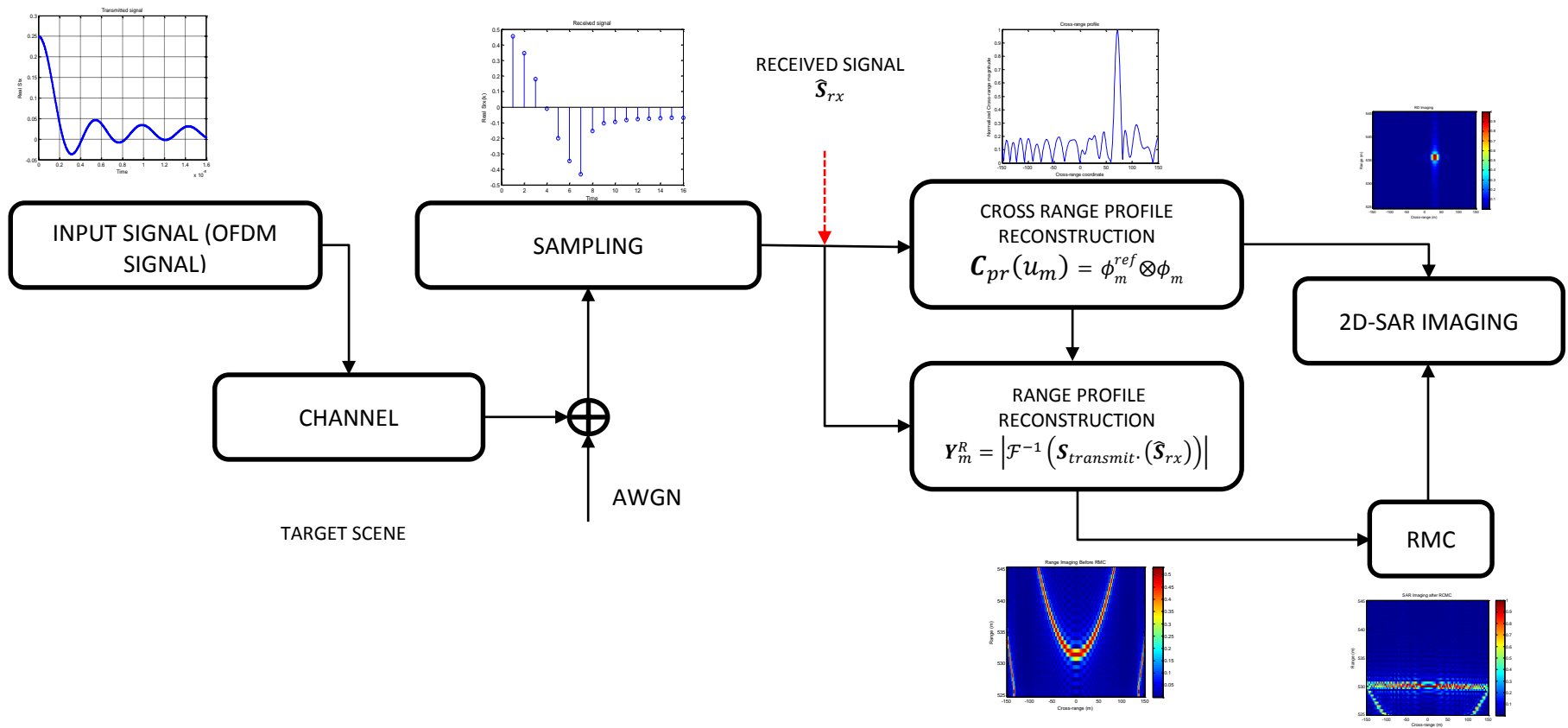


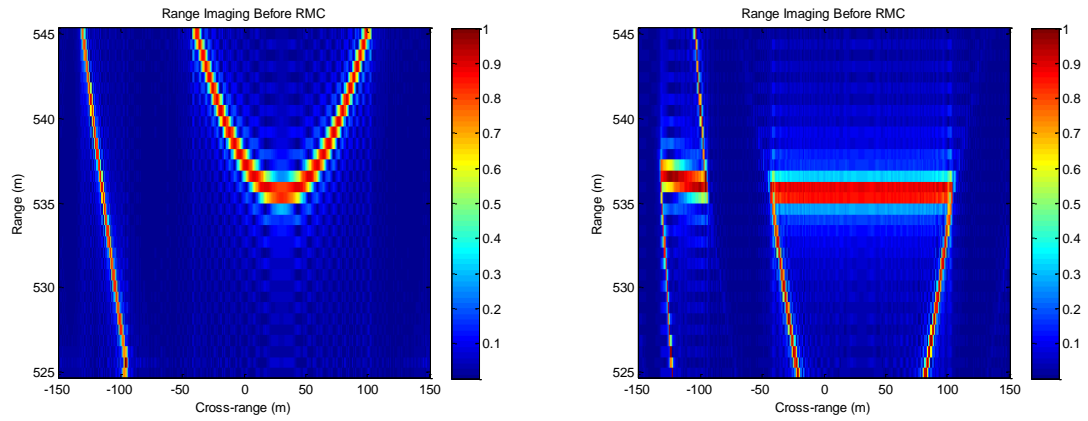
Figure 4.5 Formation of a 2D SAR Image

4.5 Simulation and Results

For the simulation, reference is made to both the single and multiple target scenarios presented in Chapter 3. Both the two scenarios were imaged using the procedure discussed in the previous sections.

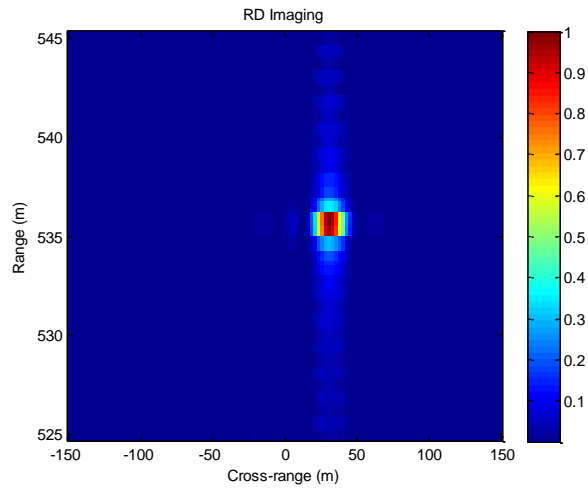
4.5.1 Single Target Imaging

For the single target imaging, we assume that the target is located at $u_0 = 30m$ and $y_0 = 535m$ and the results are shown in Figure 4.6. The images before and after RMC are shown here and after taking the product of the range and cross range profiles, the image in Figure 4.6(c) is obtained. The target position was identified, however there are some ghost targets present in the scene. This is a result of range ambiguity discussed earlier in chapter 2. Reducing the range ambiguity will surely reduce the ghost targets.



(a)

(b)



(c)

Figure 4.6 2D SAR Imaging for (a) Image before RMC. (b) Image after RMC.

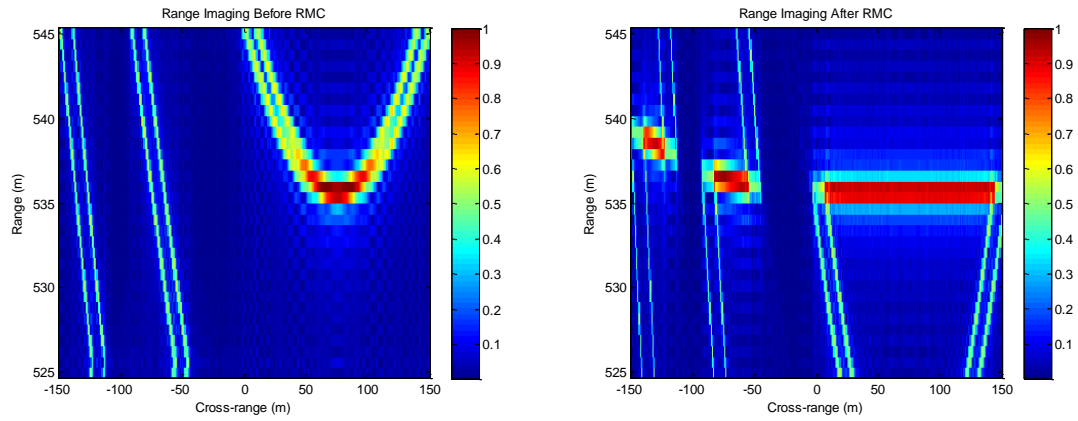
(c) Final Image

4.5.2 Multiple Targets Imaging

For the multiple target imaging, the range resolution described in chapter 3 comes into play. This is because for SAR imaging, both the cross range and range information are needed. So given a cross range resolution, δx , and range resolution, ΔR , if any of the condition $d_C \geq \delta x$ or $d_R \geq \Delta R$ is satisfied, the radar can resolve the targets, otherwise it will image them as one single target. Keeping this in mind, the following cases are considered:

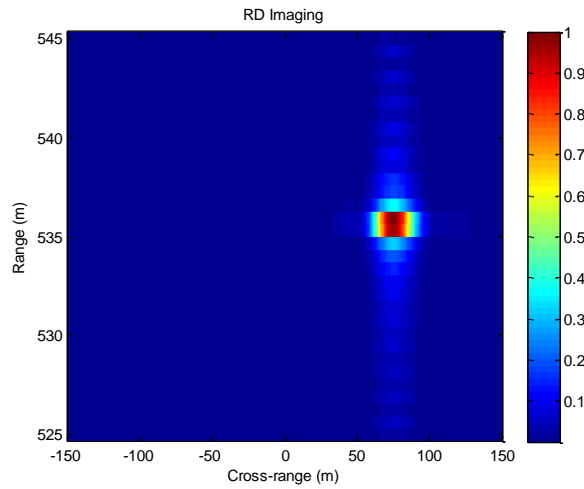
Case I: $d_C < \delta x$ and $d_R < \Delta R$:

In this case, the targets are both closely spaced to each other in range and cross range coordinates. For two targets scenario, the targets were located at $u_{o1} = 70m$, $u_{o2} = 80m$ and $N = 32$ both at a range position of $y_0 = 535m$ and image of the scene is shown in Figure 4.7. We observed that since the targets are close to each other (i.e. $d_C < \delta x$) and because of the fact that they are both at the same range, the radar imaged the two targets as one single large target extending from 70 to 80m. Also considering the case of more than two targets closely spaced to each other, the radar still images these targets as one single target as shown in Figure 4.8. In this case, the image of 15 equally weighted equidistance point like targets at cross range positions ranging between 20 to 50m all at a range position of $y_0 = 530m$ is shown as one single large target.



(a)

(b)



(c)

Figure 4.7 2D SAR Image for two targets scenario when $d_C < \delta x$ and $d_R < \Delta R$ for (a) Image before RMC. (b) Image after RMC. (c) Final Image.

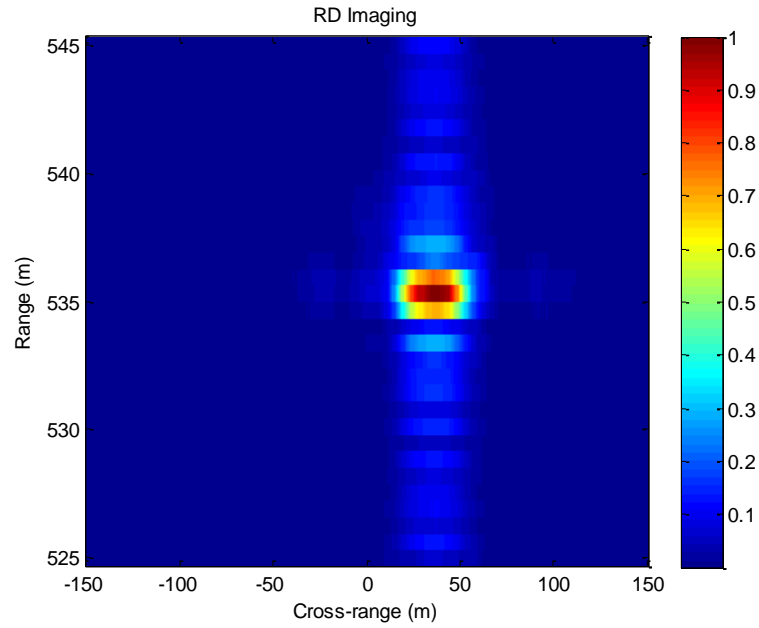
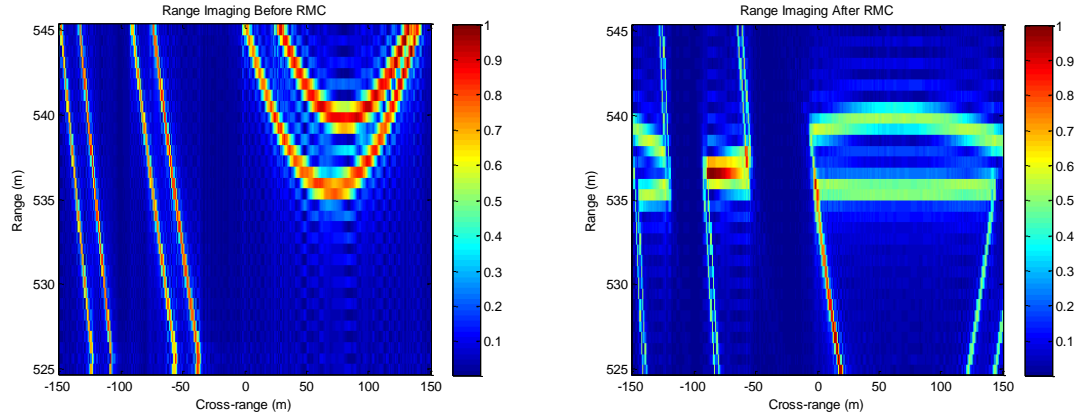


Figure 4.8 2D SAR Image for multiple targets scenario when $d_C < \delta x$ and $d_R < \Delta R$

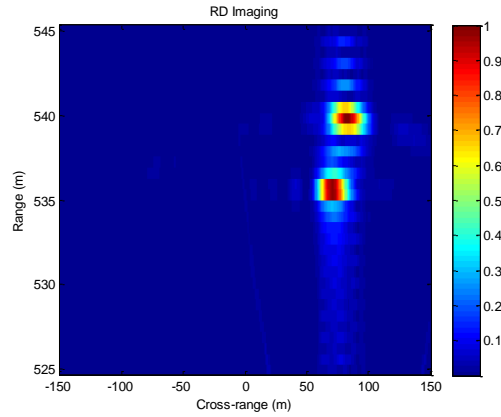
Case II: $d_C < \delta x$ and $d_R \geq \Delta R$:

When the targets are at different range positions, even though $d_C < \delta x$, the radar can successfully resolve the targets. This is because the range information helps the radar in distinguishing the targets. In this case, the two targets are located at $u_{01} = 70m$ $u_{02} = 80m$ at range positions of $y_{01} = 535m$ and $y_{02} = 540m$ respectively. The results are shown in Figure 4.9.



(a)

(b)



(c)

Figure 4.9 2D SAR Image for two targets scenario when $d_C < \delta x$ and $d_R \geq \Delta R$ for

(a) Image before RMC. (b) Image after RMC. (c) Final Image.

Case III: $d_C \geq \delta x$ and $d_R < \Delta R$:

In this case, the two targets are located at $u_{o1} = 40m$ and $u_{o2} = 90m$ and for simplicity, both targets are at the same range position of $y_0 = 535m$. This effectively makes d_R zero and hence $d_R < \Delta R$. The results are shown in Figure 4.10. It can be seen that even

though $d_R < \Delta R$, the radar successfully resolved the two targets since the condition $d_C \geq \delta x$ is met for the cross range position.

For more than two targets, four targets are considered located at cross range positions of -50, 0, 50 and 90m all located at the range position $y_0 = 535m$. The results are shown in Figure 4.11. Also, we can see that the radar successfully distinguished the targets.

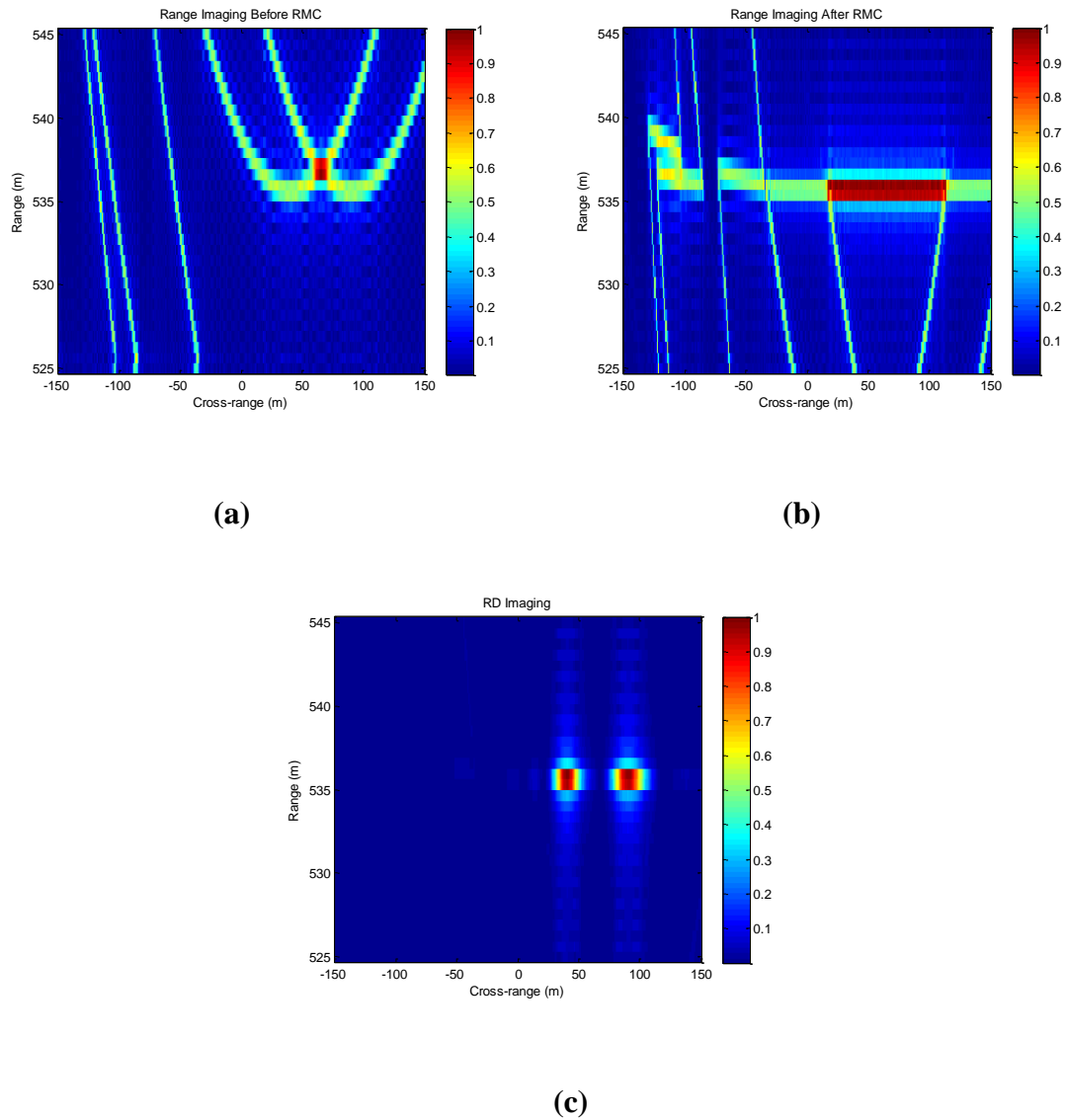


Figure 4.10 2D SAR Image for two targets scenario when $d_C \geq \delta x$ and $d_R < \Delta R$ for (a) Image before RMC. (b) Image after RMC. (c) Final Image.

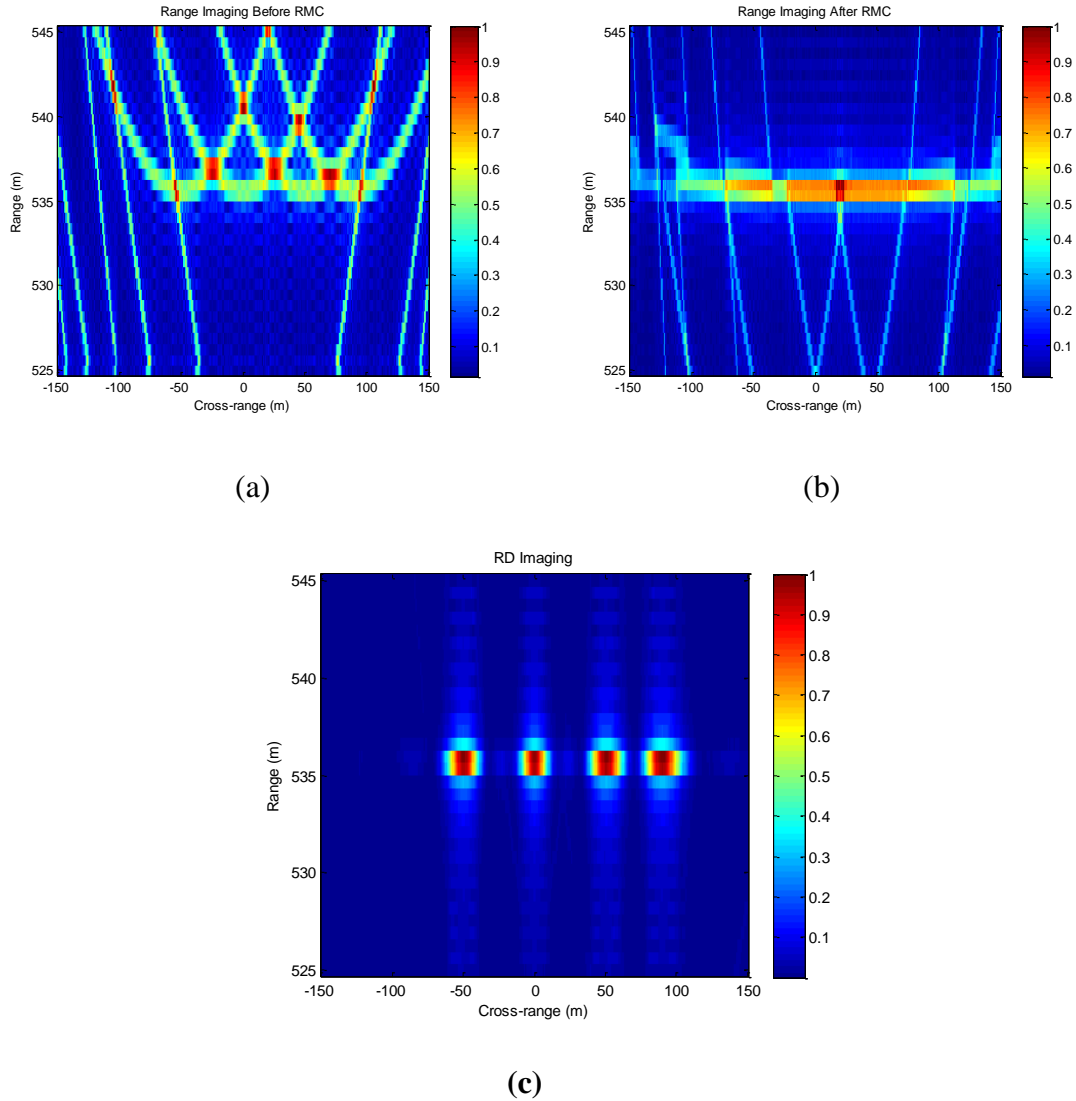


Figure 4.11 2D SAR Image for multiple targets scenario when $d_C \geq \delta x$ and $d_R < \Delta R$ for (a) Image before RMC. (b) Image after RMC. (c) Final Image.

Case IV: $d_C \geq \delta x$ and $d_R \geq \Delta R$ (Far targets):

For the two targets scenario, the targets are located at $u_{01} = 40m$ and $u_{02} = 90m$ both at range position of $y_{01} = 530m$ and $y_{02} = 540m$ respectively and the image of the scene is as shown in Figure 4.12. It can be seen that because of the fact that both conditions are

met, the radar imaged the scenes successfully distinguishing between the two targets positions. In the same vein, for the case of more than two targets, we simulated the image scene of 4 equally spaced points like targets at cross range positions of -50, 0, 50 and 90m and range positions of 540, 530, 535 and 540m respectively and the result is shown in Figure 4.13.

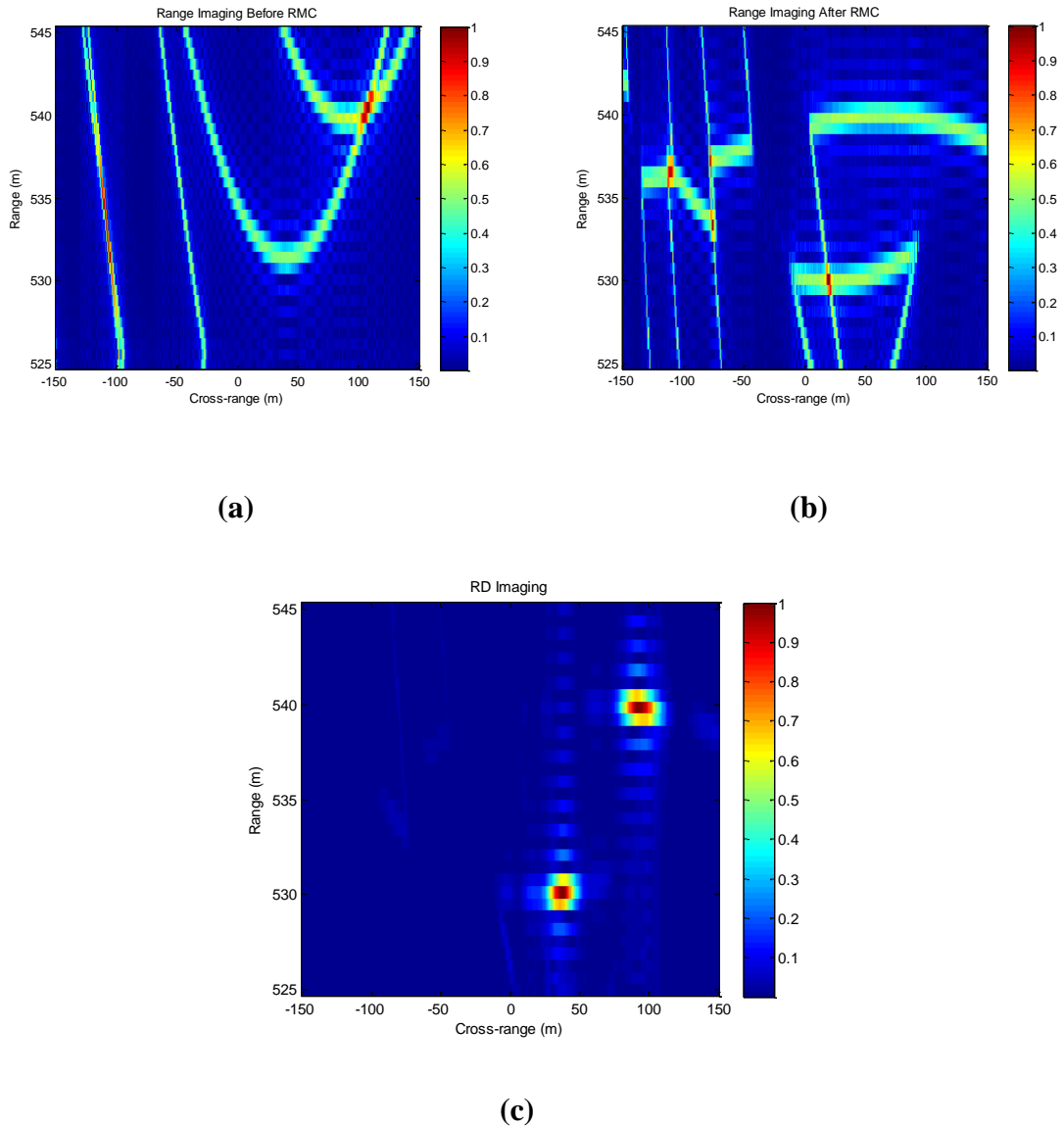


Figure 4.12 2D SAR Image for two targets scenario when $d_C \geq \delta x$ and $d_R \geq \Delta R$ for (a) Image before RMC. (b) Image after RMC. (c) Final Image.

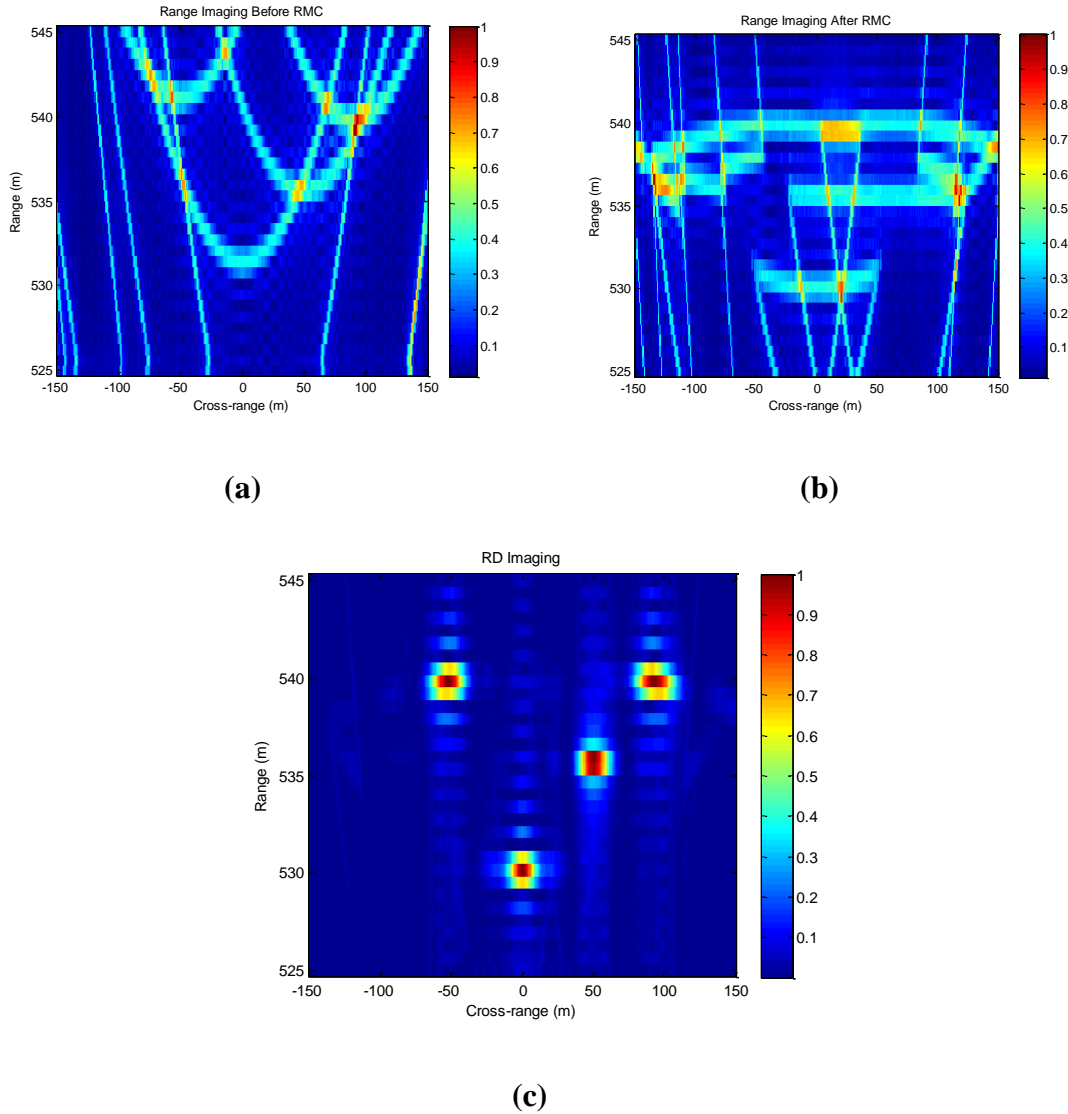


Figure 4.13 2D SAR Image for multiple targets scenario when $d_C \geq \delta x$ and $d_R \geq \Delta R$ for (a) Image before RMC. (b) Image after RMC. (c) Final Image.

From Figure 4.13, even with the presence of multiple targets, since both targets satisfy the conditions that $d_C \geq \delta x$ and $d_R \geq \Delta R$, the radar successfully distinguishes the image of each targets. However in both the two scenes, they also suffer from ghost images as a result of range ambiguity. This can be reduced by employing a system that can suppress the range ambiguity and thereby eliminating the problem of ghost images.

4.6 Chapter Summary

This chapter deals with formation of a 2D SAR image. To form a 2D SAR image, both the range and cross range profiles are needed for the image formation which can be obtained by simply taking the product of each of the RPR with the corresponding CPR. The range profile RPR suffers from two problems range migration and range ambiguity. The problem of range migration can be solved using RMC while for the range ambiguity, it depends on the choice of the OFDM subcarriers whether random or uniform assignment of the subbands and this reduce the ambiguity in the range significantly. Range ambiguity is among the factors responsible for the appearance of ghost images in the scene. Moreover, two cases for the imaging were considered namely single and multiple targets imaging. For both cases, the image were reconstructed successfully although some ghost images were visible. However for the multiple targets imaging, either of the condition $d_C \geq \delta x$ or $d_R \geq \Delta R$ need to be satisfied for the radar to distinguish between images from different targets otherwise it will image them as one single large image.

CHAPTER 5

OFDM WAVEFORM DESIGN FOR RANGE

AMBIGUITY SUPPRESSION

5.1 Introduction

In this chapter, we investigate the impacts of choosing the OFDM signal vector \mathbf{S} in range ambiguity suppression. It has been established that there is always a tradeoff between making a random and uniform assignment of sub-bands. Making a uniform assignment of the sub-bands gives better imaging results but the transmitted signal becomes vulnerable and easily identifiable if intercepted. However choosing the sub-bands randomly makes the range side lobes higher and as a result degrades the system performance. So the problem is how to assign the N sub-bands efficiently to satisfy both requirements. In the following sections, we will see how this is possible.

5.2 Factors Affecting the Choice of OFDM Signal Vector \mathbf{S}

In order to make a decision on choosing the OFDM signal vector \mathbf{S} (random assignment of the sub-bands), several factors need to be considered that can affect our choice. These factors are as follows:

- i. Presence of narrowband interference, jamming, noise or both. A noisy channel will definitely affect the choice of the N sub-bands . This was clearly shown in Chapter 3 whereby if we have a low SNR, N has to be small and vice versa.
- ii. Reflectivity of the target: The frequency dependence of the target reflectivity coefficient also affects the choice of the sub-bands .
- iii. Environmental platform: The platform we are operating can also affect the choice of the sub-bands significantly and as such we need to know if the environment we are operating can coexist with other friendly platforms. This is important because of co-channel interference.
- iv. Tradeoff between N and subcarrier symbol time: As a rule of thumb, the more subcarriers used, the longer their symbol rate even though the overall rate of information remains the same for a lower and higher value of N , a longer symbol rate is desirable in multipath mitigation. Therefore subcarrier spacing is a necessary parameter to choose for an OFDM signal.

5.3 Impact of Choosing S Randomly

In chapter 3, we presented the results for both the case of uniform and random assignments of the N sub-bands . For convenience, the results of the RMSE are presented here again in Figure 5.1. For the case of uniform assignment of the N sub-bands (all sub-bands are ON), the result gives a better performance because the side lobes are very low as a result of using uniform sub-bands . But in practice, using a uniform assignment of the sub-bands will make the transmitted signal vulnerable and easily intercepted and hence the need to randomize the sub-bands . A random assignment of sub-bands makes the transmitted signal

almost impossible to be read even when detected but the side lobes levels becomes higher which degrades the performance of the system. Because of this tradeoff, a compromise is needed to investigate the choice of the OFDM signal that will give a good performance and difficult to be identified when intercepted.

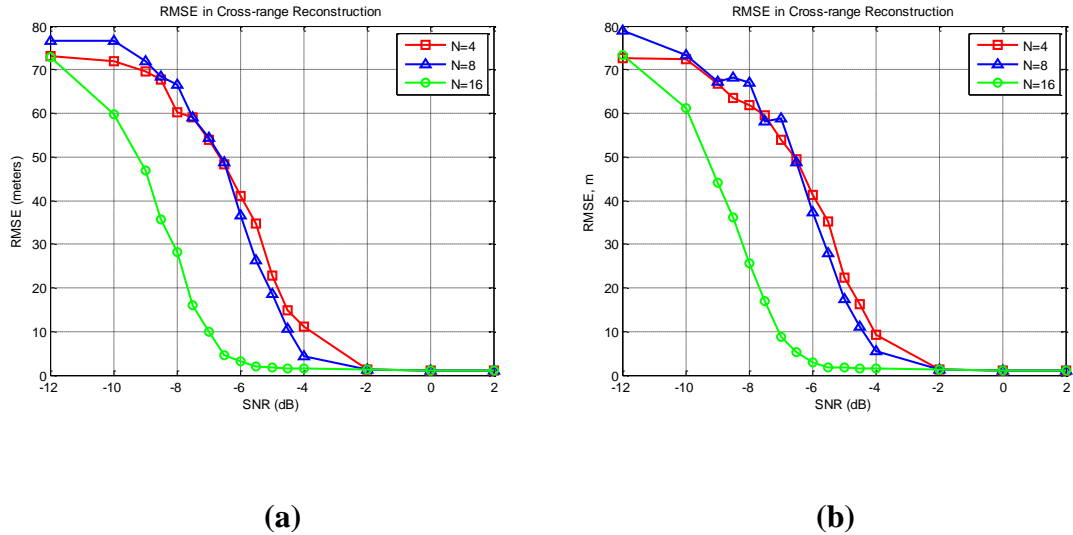


Figure 5.1 RMSE for (a) Uniform assignment of the sub-bands. (b) Random assignment of the sub-bands.

5.4 Adaptive Design of OFDM subcarrier N

From Figure 5.1, it has been shown that the RMSE improves as the SNR increases. Also three regions of operation can be identified namely between $-20dB$ to $-12dB$, $-12dB$ to $-2dB$ and above $-2dB$ and as such N can be made to adapt to the best value of N that gives a better performance. To show this adaptation scenario clearly, the RMSE result of Figure 5.1 is extended to cover the region between $-20dB$ to $2dB$ and the result is shown in Figure 5.2. It is observed that between $-20dB$ to $-12dB$ (the noisy region) $N = 4$ gives the

best performance in terms of RMSE than either $N = 8$ or $N = 16$ and therefore the adaptive N choose the value of $N = 4$. However it is uncommon and nobody will like to operate at an error of $70m$. From $-12dB$ to $-2dB$, $N = 16$ gives a better performance compared to $N = 4$ and $N = 8$ and as such the adaptive N chooses this path. Above $-2dB$, this region is notably good and therefore any value of N can be chosen depending on the application in consideration. Therefore, an additional plot is added called Adaptive N which indicate the best choice of N in every region.

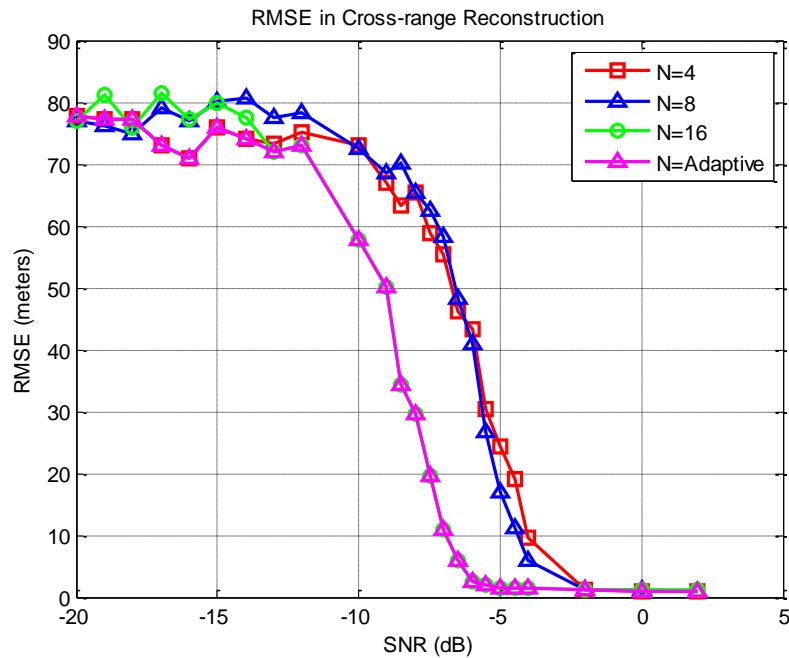


Figure 5.2 RMSE for Uniform assignment of the sub-bands with Adaptive N .

5.5 Design of OFDM Waveform in Range Ambiguity Suppression

As stated earlier in this chapter, fully random assignment of subcarrier coefficients result in high range side lobes while uniform assignment of this subcarrier coefficients result in

lower range side lobes but this can only be employed in a friendly environment. In a hostile environment such as military applications where much emphasis is given to the design of the transmitted signal so that it is almost impossible to be identified even when intercepted, we cannot transmit uniform subcarrier coefficients. Moreover, the system needs to be as accurate as possible. To start with, there are several ways to approach this problem. One possible approach is to maintain the uniform assignment of the sub-bands and modulate it with a sequence of random numbers but the sequences must have a lower cross correlation values to provide degradation of false targets. Hence PN sequences (such as Gold and Kasami) can be used for this purpose. So even if the signal is intercepted, it cannot be easily decoded. At the receiver end, the received signal is demodulated to get the original transmitted signal. A second approach is to design a coding scheme that will make half of the transmitting sequence uniform and the other half random. These two design processes are discuss in the coming sections.

5.5.1 Uniform/Random Coding

Uniform/random coding means to design a code in which half of the sub-bands are ON (ones) called uniform assignment of the sub-bands and the other half of the sub-bands are ON and OFF (consisting of equal number of zeroes and ones) called random assignment of the sub-bands. This system of code design will help us find a compromise between uniform and random assignment of the subcarrier coefficients without additional costs and still achieve the intended result. To do this, the code is divided into four parts and let the uniform assignment of the code be α and the random assignment be β . So given a coding scheme \mathbf{C} of length equal to the length of the sub-bands N , we can divide \mathbf{C} into four parts consisting of α and β given by

$$\mathbf{C} = \alpha\beta\alpha\beta \quad (5.1)$$

where N is the length of \mathbf{C} and the code length of each of α and β is $N/4$. By concatenating these codes together (α and β), we will get back the original size of \mathbf{C} . Considering all the possible combinations of α and β , a code in which half of it is uniform and half of it is random can be achieved and also get acceptable range side lobes that are in agreement with the results obtained previously using uniform subcarrier assignment. Table 5.1 shows all of the possible combinations of α and β .

Table 5.1 Possible Combinations of α and β

n	Possible Combinations
1	$\alpha\alpha\beta\beta$
2	$\alpha\beta\alpha\beta$
3	$\alpha\beta\beta\alpha$
4	$\beta\alpha\alpha\beta$
5	$\beta\alpha\beta\alpha$
6	$\beta\beta\alpha\alpha$

From Table 5.1, we have six possible combinations to generate the uniform/random codes all of which have a lower range side lobes compared to the fully random assignment of the sub-bands although the degree of randomness is not as immune as the fully random case. To simulate this coding scheme, the same parameters are used as the ones in chapter 4. So N is chosen to be 32 ($N = 32$) and all other parameters remain the same. A typical image for full random assignment of the sub-bands is shown in Figure 5.3. The target is located at (0m, 535m) and it can be seen that it is almost impossible to tell where exactly the target

is in the scene. For the uniform/random coding, two imaging scenarios of single and two targets are consider and the results are shown in Figure 5.4. For the single target, the target is located at (40m, 530m) and for the two targets scenario, the other target is located at (90m, 540m).

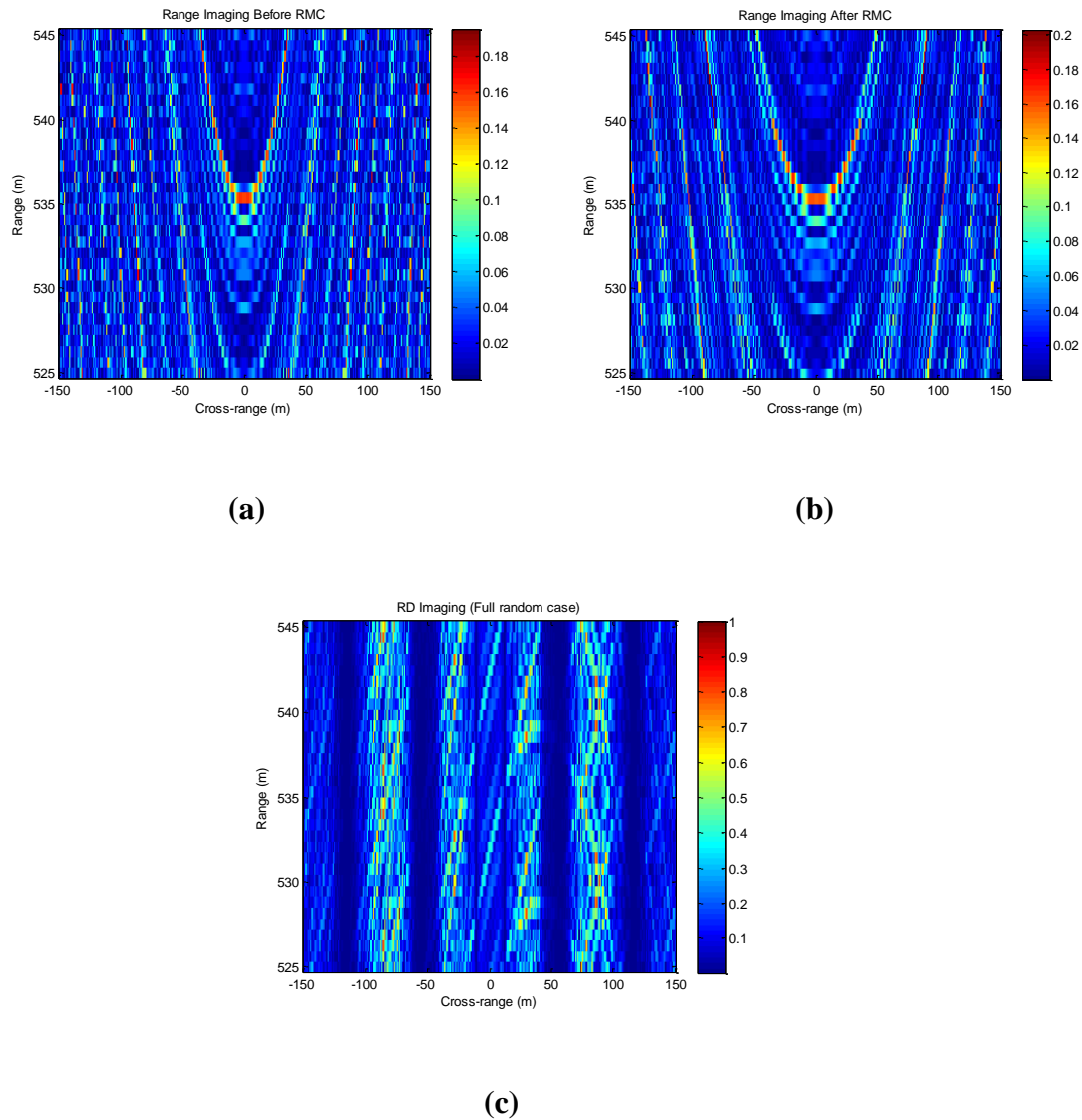


Figure 5.3 2D SAR Imaging for full random assignment of the sub-bands (a) Image before RMC. (b) Image after RMC. (c) Final Image.

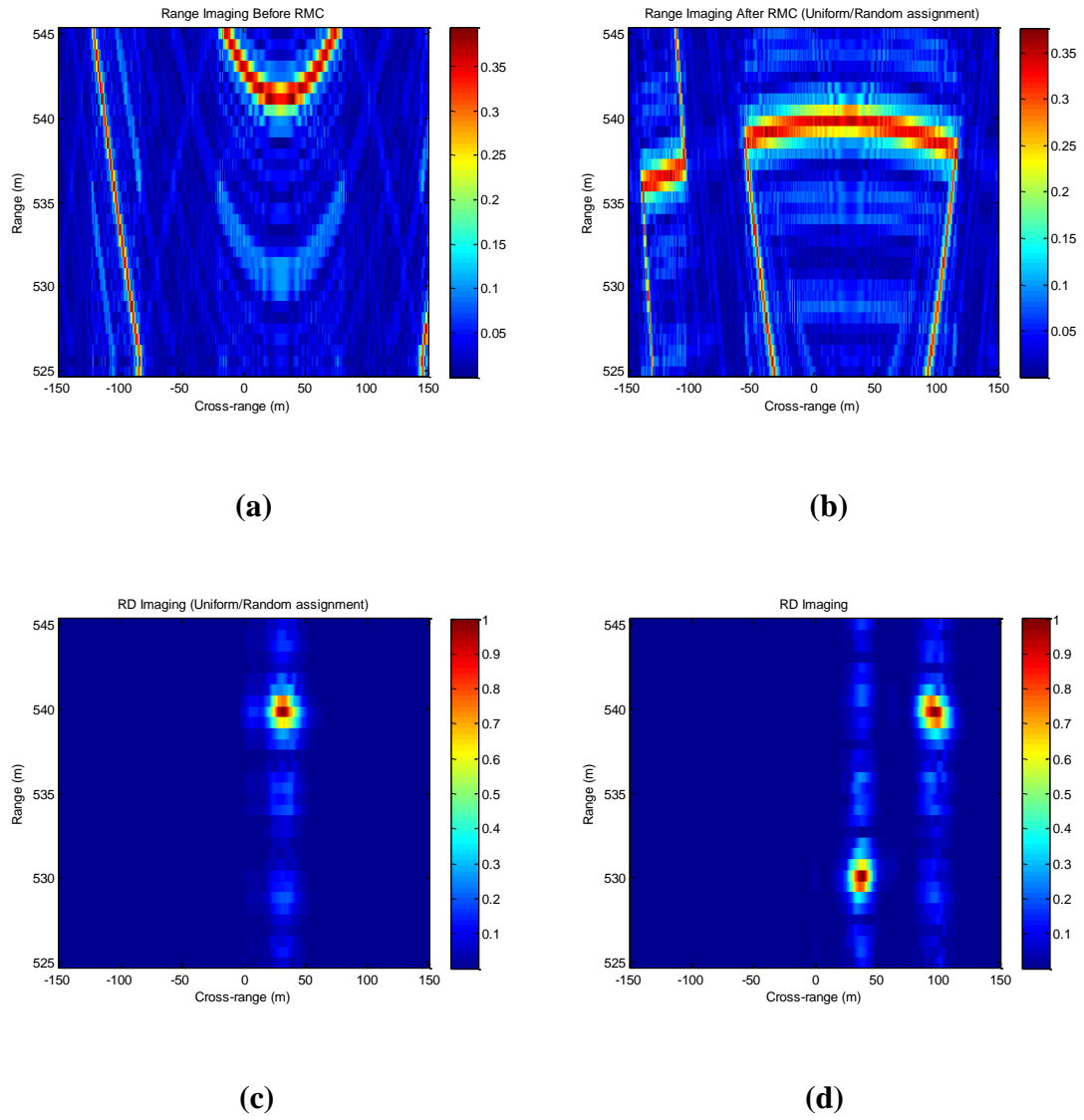


Figure 5.4 2D SAR Imaging for uniform/random assignment of the sub-bands (a) Image before RMC. (b) Image after RMC. (c) Final Image for single target. (d) Final Image for two targets.

From Figure 5.4, it can be observed that by employing the method of uniform/random assignment of the sub-bands, we can identify the position of the target in the scene and therefore shows the capability of the technique in comparison to full random assignment of the sub-bands.

5.5.2 Pseudo-Noise (PN) Sequences

PN sequences are binary sequences that exhibit the characteristics of noise like random sequences. For any PN sequences to achieve this degree of randomness, they must satisfy three randomness properties namely balance, run and shift property as postulated by Golomb [39]. In addition to these properties, to analyze a PN sequence used in CDMA/OFDMA applications the following properties need to be defined:

- I. Cross Correlation Function (CCF): This is a measure of similarity between two different sequences which can be expressed using

$$R_x(k, l) = \sum_{i=1}^n (2b_{ik} - 1)(2b_{il} - 1), \quad 0 \leq j \leq n - 1 \quad (5.2)$$

where b_{ik} and b_{il} are the coefficients of the sequence for the different signals to be considered within the period n .

- II. Auto Correlation Function (ACF): This is an impulse response to suppress multipath (i.e. self-interference) and it is the measure of similarity between the sequence and its cyclic shifted copy which can be obtained from equation (5.2) by making $k = l$.

Waveforms are analyzed in terms of their ACF and CCF. The ACF and CCF properties of any sequences used in generating the transmitted signal play a significant role in SAR imaging and also in detecting false target rejection. In essence, sequences that give better ACF properties provide high resolution in target detection and lower CCF properties provide degradation of false targets. So the objective here is to find a sequence that provides the lowest cross correlation and higher autocorrelation properties among all the sequences used.

Given a data signal $s_t(t)$ transmitted at frequency f and a PN sequence $PN(t)$ at a frequency of f_c , the transmitted signal is given by

$$s(t) = s_t(t)PN(t) \quad (5.3)$$

$s(t)$ is sent through the channel and get reflected back. At the receiver end, the received signal is correlated with $PN(t)$ and the original message will be recovered under the assumption that there is perfect synchronization between the transmitted and the received sequences. If $r(t)$ denote the received signal, the recovered signal will be

$$s_t(t) = r(t)PN(t) \quad (5.4)$$

A diagrammatic representation of this process is shown in Figure 5.5.

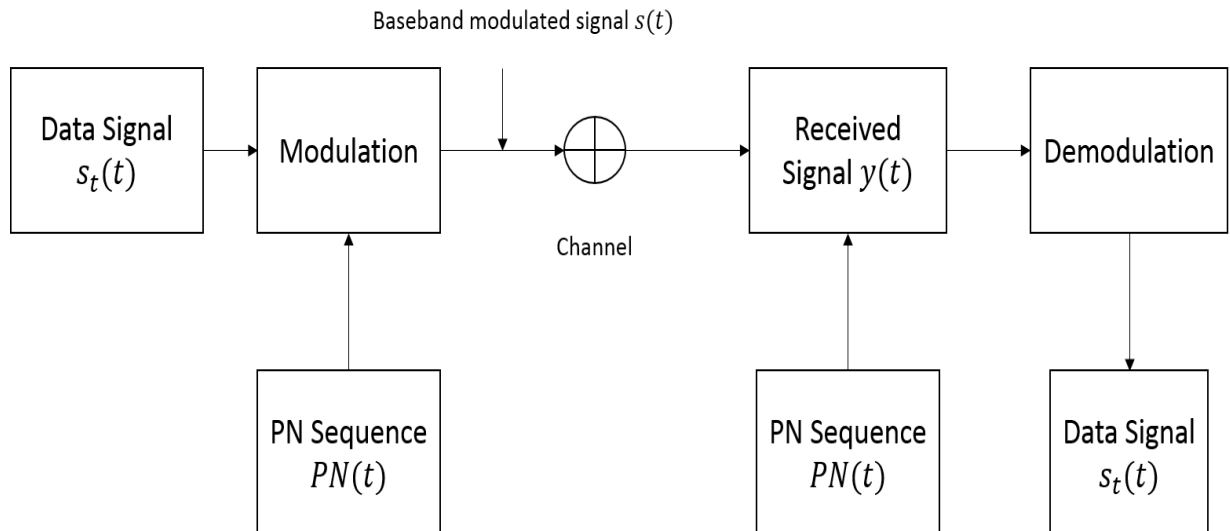


Figure 5.5 Transmission and reception process using PN Sequences.

There are different kinds of PN sequence families such as the maximum-length shift register (m-sequences), Walsh-Hadamard codes, Gold sequence codes and Kasami codes. However among these family of codes, we are interested in the ones that will give us a lower CCF and higher ACF and base on this consideration, only Gold and Kasami codes satisfies these requirements. So our next discussion will be on these two coding schemes.

5.5.3 Gold Sequences

Given a preferred pair of sequences of period $n = 2^m - 1$, we can generate a new family of sequences by taking modulo-2 sum between the pair of sequences. The resulting sequences are called Gold sequences. These sequences exhibit a 3-values CCF with values given by $\{-1, -t(m), t(m) - 2\}$, where $t(m)$ is given by [40]

$$t(m) = \begin{cases} 2^{(m+1)/2} + 1 & \text{odd } m \\ 2^{(m+2)/2} + 1 & \text{even } m \end{cases} \quad (5.5)$$

To generate a Gold sequence, two PN sequences namely sequence 1 and sequence 2 are combine using exclusive OR (XOR) and the resultant output is the preferred Gold sequence as shown in Figure 5.6. The values of these sequences can be determined from Table 5.2 which shows the list of preferred pairs of PN sequences that can be used to generate the Gold sequences. For our case, $m = 5$ so from the Table 5.2, we use the sequence [5 2 0] and [5 4 3 2 0] as sequence 1 and sequence 2 respectively.

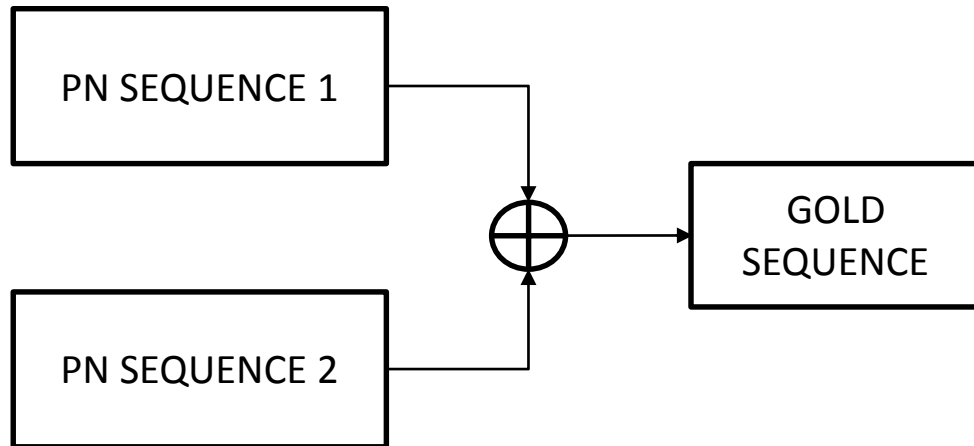


Figure 5.6 Generation of a Gold Sequences

Table 5.2 Preferred pairs of PN sequences to generate Gold sequence

m	n	SEQUENCE 1	SEQUENCE 2
5	31	[5 2 0]	[5 4 3 2 0]
6	63	[6 1 0]	[6 5 2 1 0]
7	127	[7 3 0]	[7 3 2 1 0]
9	511	[9 4 0]	[9 6 4 3 0]
10	1023	[10 3 0]	[10 8 3 2 0]
11	2047	[11 2 0]	[11 8 5 2 0]

However one of the draw backs of Gold sequences is it inability to operate within the lower bound set by Welch bound which stated that given M number of sequences of length n and m number of stages in the shift register, the maximum cross correlation is given by

$$R_{max} \sqrt{\frac{M-1}{Mn-1}} = n \sqrt{\frac{M-1}{n(M-\frac{1}{n})}} \approx \sqrt{n} \text{ for large values of } M \text{ and } n \quad (5.6)$$

This motivates the use of Kasami codes.

5.5.4 Kasami Sequences

Kasami codes are optimal in terms of cross correlation as they achieve or operate within the Welch bound but they generate a smaller set of codes. Their ACF and CCF take on values from the set $\{-1, -(2^{m/2} + 1), 2^{m/2} - 1\}$. Hence the maximum cross correlation value for any pair of sequences from the set is

$$R_{max} = 2^{m/2} + 1 \quad (5.7)$$

So these PN sequences enable us to use a uniform code or a code with weak randomization in hostile environment without the fear of being decoded when intercepted. At the receiver end, we just multiply with this PN sequence and get our data back. This technique performs the same way with uniform assignment of the sub-bands .

To simulate this coding scheme, the same parameters are used as the case of uniform/random coding and two imaging scenario of single and two targets are consider and the results are shown in Figure 5.7 and Figure 5.8. For the single target, the target is located at (20m, 535m) and for the two targets scenario, the other target is located at (70m, 530m). It can be seen that the results behaves in similar way with uniform assignment of the sub-bands (i.e. all the sub-bands are ON). Table 5.3 shows the parameters used for the

simulation. Both codes are generated using MATLAB following the description outlined in the text.

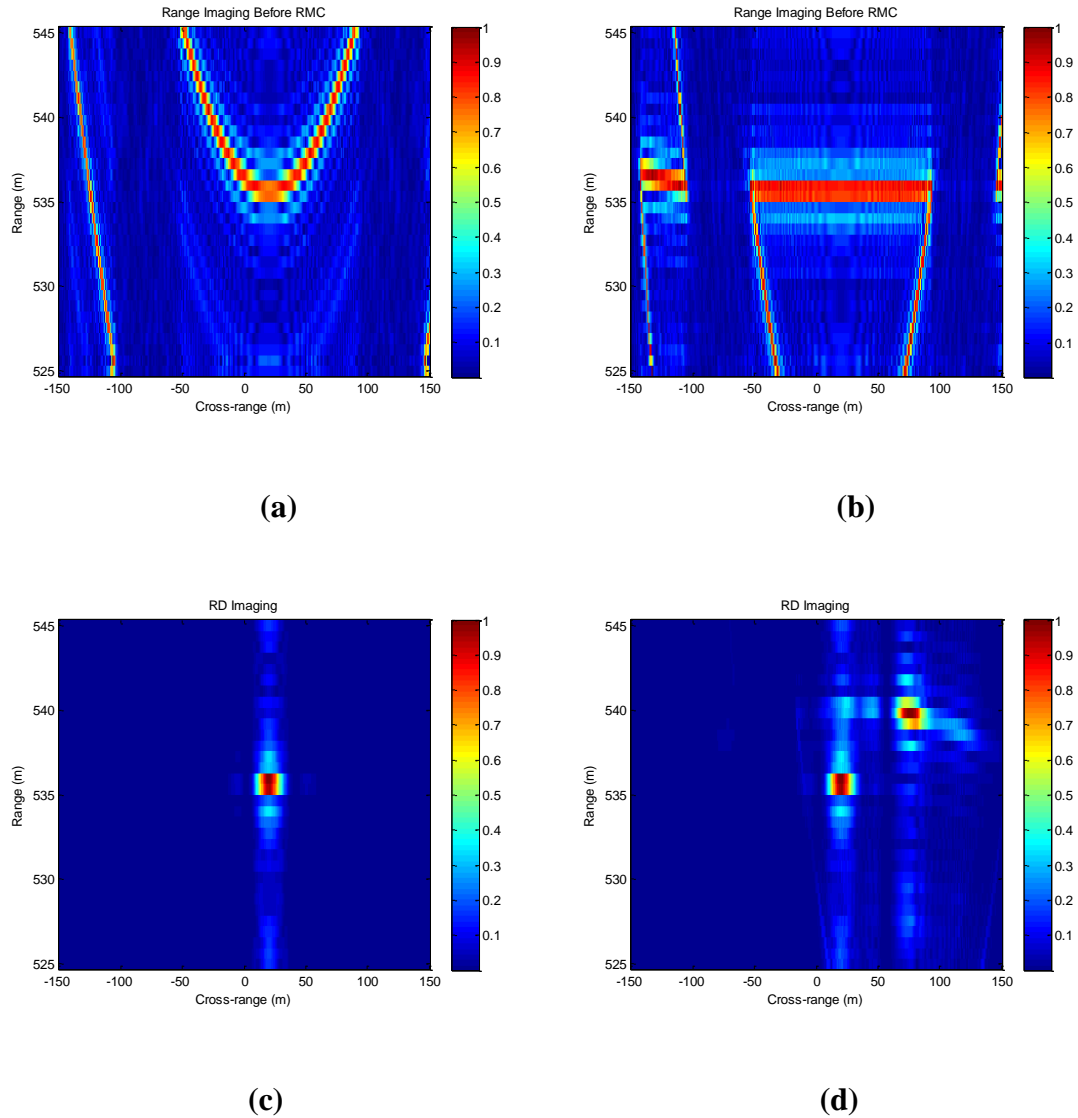
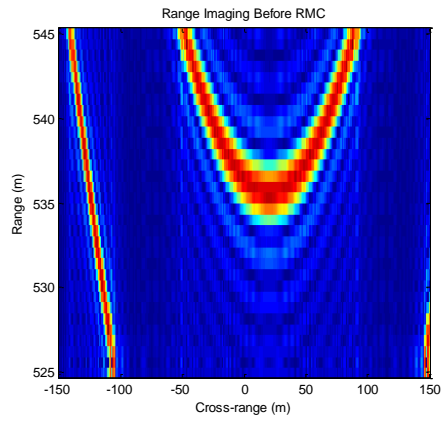
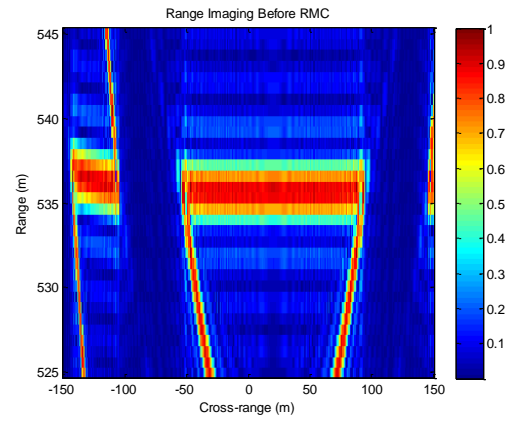


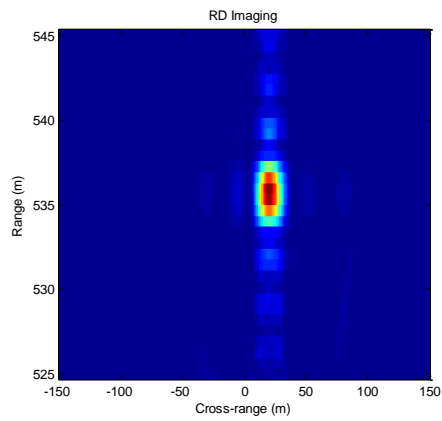
Figure 5.7 2D SAR Imaging using Gold codes (a) Image before RMC. (b) Image after RMC. (c) Final Image for single target. (d) Final Image for two targets.



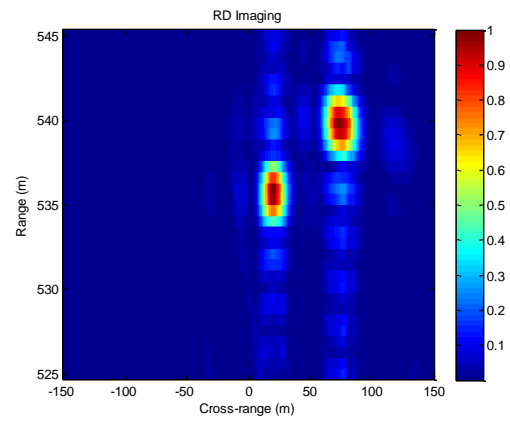
(a)



(b)



(c)



(d)

Figure 5.8 2D SAR Imaging using Kasami codes (a) Image before RMC. (b) Image after RMC. (c) Final Image for single target. (d) Final Image for two targets.

Table 5.3 Values of the codes used for the simulation

CODE TYPE	CODE
Uniform codes (All sub-bands ON)	[111111111111111111111111111111111111]
Gold Sequence	[11100000010010000110100110100101]
Kasami sequence	[00100101010101100011101010011001]

5.6 Chapter Summary

This chapter deals with the factors affecting the choice of subcarrier coefficients vector in range ambiguity suppression and how to design an OFDM waveform to overcome such challenges. An investigation on the impact of uniform and random assignment of the sub-bands was carried out. To achieve a lower range side lobes, uniform assignment of the sub-bands is preferable however it is only applicable in friendly environment. In hostile environment, random assignment of the sub-bands is desirable but it has the problem of having high range side lobes. Because of this issue, we design an OFDM waveform using uniform/random assignment of the sub-bands and PN sequences. For the uniform/random assignment of the sub-bands, it was shown that it is possible to design a code that has an acceptable range ambiguity (range side lobes). PN sequences however provide us with a way to use uniform assignment of the sub-bands in hostile environment by modulating the data to be transmitted with a PN sequence. At the receiver end, we demodulate the received signal to get back the message sent.

CHAPTER 6

SUMMARY AND CONCLUSIONS

In this thesis, we investigated the use of UWB OFDM signals in SAR cross range reconstruction and SAR imaging for single and multiple targets. At first, a single target model was assumed and later extended to multiple targets. Issues associated with range profile such as the problem of range migration and how to correct it using RMC, range ambiguity and how to efficiently design an OFDM waveform to suppress the high range side lobes were discussed. So this chapter concludes the thesis work and give recommendations for possible future work.

6.1 Conclusions

The thesis focus on the use of UWB OFDM signals in SAR signal processing for both single and multiple targets models. Starting with a single target, the CPR was reconstructed via matched filtering of the estimated phase history with a reference function in time domain. Parameters such RMSE, cumulative side lobe level and the main lobe width were used to test the accuracy of the reconstructed CPR. We also looked at the effect of varying the step interval of the phase history grid search using different number of subcarriers in target location. It was shown that as the number of subcarriers increases, the accuracy of the reconstructed CPR improves, however we pay the price of having a wider main lobe of the CPR. Therefore an optimal number of subcarriers for the OFDM signal is needed for this approach to be effective.

Also we observed that for different values of N , the grid search for the phase history behaves in a different way. Whereas the estimation of the reconstructed CPR improves by decreasing the step interval $\Delta\beta$ for the case of $N = 4$, the reverse is the case for $N = 8$ and almost has no effect when $N = 16$. For $N = 16$, we had enough data available for estimation.

For the multiple targets, we presented the necessary conditions for the radar to distinguish echoes received from different targets. These conditions are cross range resolution and range resolution. Once the echoes received satisfied any of these conditions, the receiver can distinguish the different target positions otherwise it will image them as one single large target. At the receiver end, the received signal is found by taking the superposition of the individual echoes from different targets. Moreover, as we have many targets present, the probability of making error in the position of the target increases. This probability of error is known as probability of false alarm and it can be taken care of by setting a threshold level of which each response from the target has to reach before it can be recorded as target position otherwise it is assumed to be a false alarm and will be discarded.

In the SAR image formation, the CPR and RPR information were combined by taking the product between each of the RPR with the corresponding CPR value. But before using the RPR, RMC was performed on the range to correct the effect of range migration as a result of the movement of the radar. We have also seen that for the model to be used both in friendly and hostile environment, a code was designed to suppress the ambiguity associated with the range and make the code impossible to be identified even when it is intercepted. This coding scheme was designed using uniform/random assignment of the subcarrier vector and PN sequences (Gold and Kasami codes).

6.2 Future work

Based on the work presented in this thesis, there are still possible additions to this work in order to make it more effective. The following areas are possible additions:

- I. Extending the work to include the possibility of using compressive sensing to compress the OFDM waveform.
- II. The work can also be extended by using a non AWGN channel such as Rayleigh.
- III. The use of UWB OFDM in Through the Wall Radar Imaging (TWI).
- IV. Looking at the potential challenges of practical implementation of UWB OFDM SAR, such as high Peak-to-Average Power Ratio (PAPR), Inter Carrier Interference (ICI) and sensitivity to Doppler shifts which may damage the OFDM subcarriers' orthogonality.

REFERENCES

1. Schuerger, J. and D. Garmatyuk. *Performance of random OFDM radar signals in deception jamming scenarios*. in *Radar Conference, 2009 IEEE*. 2009.
2. Schuerger, J.P., *Ultra-Wideband OFDM Radar and Communication System*, in *Department of Physics*2009, Miami University: Oxford, Ohio. p. 80.
3. Garmatyuk, D. and M. Brenneeman, *Adaptive Multicarrier OFDM SAR Signal Processing*. *Geoscience and Remote Sensing, IEEE Transactions on*, 2011. **49**(10): p. 3780-3790.
4. Dastgir, N., *Processing SAR data using Range Doppler and Chirp Scaling Algorithms*, in *School of Architecture and Built Environment*2007, Royal Institute of Technology (KTH) 100 44 Stockholm, Sweden. p. 40.
5. McDonough, J.C.C.a.R.N., *Synthetic Aperture Radar System and Signal Processing*. 1991, John Wiley & Sons, New York.
6. Mir, M.C., *Image formation for Synthetic Aperture Radar using MATLAB*, 2008, North East Wales Institute of Higher Education: Wales.
7. Mahafza, B.R., *Radar Systems Analysis and Design Using MATLAB*. 2000: CRC Press, Inc.
8. Xuehua, J. and C. Peijiang, *Research and Simulation of MIMO-OFDM Wireless Communication System*, in *Proceedings of the 2009 International Forum on Information Technology and Applications - Volume 01*2009, IEEE Computer Society. p. 83-86.
9. Kim, Y.M., *Ultrawideband (UWB) Technology and Applications*, 2003, <http://www.educyclopedia.karadimov.info/library/ultra-wide-band-kimyoung-2003.ppt>: Online.
10. Richards, M.A., *Fundamentals of radar signal processing : [state-of-the-art Fourier analysis techniques ; target and interference models ; synthetic aperture imaging ; adaptive array processing]*. 2005, New York, NY [u.a.]: McGraw-Hill.

11. Hossain, M.A., et al. *Adaptive UWB-OFDM Synthetic Aperture Radar*. in *Electronics, Communications and Photonics Conference (SIEPCPC), 2011 Saudi International*. 2011.
12. de Wit, J.J.M., A. Meta, and P. Hoogeboom, *Modified range-Doppler processing for FM-CW synthetic aperture radar*. *Geoscience and Remote Sensing Letters*, IEEE, 2006. **3**(1): p. 83-87.
13. Wen-Qin, W., P. Qicong, and C. Jingye, *Waveform-Diversity-Based Millimeter-Wave UAV SAR Remote Sensing*. *Geoscience and Remote Sensing*, IEEE Transactions on, 2009. **47**(3): p. 691-700.
14. Krieger, G., N. Gebert, and A. Moreira, *Multidimensional Waveform Encoding: A New Digital Beamforming Technique for Synthetic Aperture Radar Remote Sensing*. *Geoscience and Remote Sensing*, IEEE Transactions on, 2008. **46**(1): p. 31-46.
15. Gebert, N., G. Krieger, and A. Moreira, *Multichannel Azimuth Processing in ScanSAR and TOPS Mode Operation*. *Geoscience and Remote Sensing*, IEEE Transactions on, 2010. **48**(7): p. 2994-3008.
16. Setlur, P., M. Amin, and F. Ahmad, *Multipath Model and Exploitation in Through-the-Wall and Urban Radar Sensing*. *Geoscience and Remote Sensing*, IEEE Transactions on, 2011. **49**(10): p. 4021-4034.
17. Setlur, P., et al., *Target Localization with a Single Sensor via Multipath Exploitation*. *Aerospace and Electronic Systems*, IEEE Transactions on, 2012. **48**(3): p. 1996-2014.
18. Levanon, N., *Multifrequency complementary phase-coded radar signal*. *Radar, Sonar and Navigation*, IEE Proceedings -, 2000. **147**(6): p. 276-284.
19. Ruggiano, M. and P. Van Genderen. *Radar and communication waveform: Wideband ambiguity function and narrowband approximation*. in *Radar Systems, 2007 IET International Conference on*. 2007.
20. Sen, S. and A. Nehorai, *Target Detection in Clutter Using Adaptive OFDM Radar*. *Signal Processing Letters*, IEEE, 2009. **16**(7): p. 592-595.

21. Sen, S. and A. Nehorai, *Adaptive Design of OFDM Radar Signal With Improved Wideband Ambiguity Function*. Signal Processing, IEEE Transactions on, 2010. **58**(2): p. 928-933.
22. Soumekh, M., *SAR-ECCM using phase-perturbed LFM chirp signals and DRFM repeat jammer penalization*. Aerospace and Electronic Systems, IEEE Transactions on, 2006. **42**(1): p. 191-205.
23. Garmatyuk, D.S. *Simulated Imaging Performance of UWB SAR Based on OFDM*. in *Ultra-Wideband, The 2006 IEEE 2006 International Conference on*. 2006.
24. Yang, Z.-g., X.-t. Huang, and Z.-m. Zhou. *Multiresolution feature extraction in target detection of UWB SAR*. in *Synthetic Aperture Radar, 2007. APSAR 2007. 1st Asian and Pacific Conference*. 2007.
25. Chang, Y.-l., et al. *Moving target focusing and parameter estimation based on ROI of multi-channel UWB SAR images*. in *Signal Processing, 2008. ICSP 2008. 9th International Conference on*. 2008.
26. Kauffman, K., D. Garmatyuk, and J. Morton. *Efficient sparse target tracking algorithm for navigation with UWB-OFDM radar sensors*. in *Aerospace & Electronics Conference (NAECON), Proceedings of the IEEE 2009 National*. 2009.
27. Kauffman, K., et al. *Enhanced feature detection and tracking algorithm for UWB-OFDM SAR navigation*. in *Aerospace and Electronics Conference (NAECON), Proceedings of the 2011 IEEE National*. 2011.
28. Hossain, M.A., et al. *Anti-jamming Capabilities of UWB-OFDM SAR*. in *Radar Conference (EuRAD), 2011 European*. 2011.
29. Hossain, M.A., I. Elshafiey, and M.A. Alkanhal. *High-resolution and jamming-resistant UWB-OFDM SAR imaging*. in *Signal Processing and Information Technology (ISSPIT), 2011 IEEE International Symposium on*. 2011.
30. Wen-Qin, W., *Space-Time Coding MIMO-OFDM SAR for High-Resolution Imaging*. Geoscience and Remote Sensing, IEEE Transactions on, 2011. **49**(8): p. 3094-3104.
31. Garmatyuk, D., *Cross-Range SAR Reconstruction With Multicarrier OFDM Signals*. Geoscience and Remote Sensing Letters, IEEE, 2012. **9**(5): p. 808-812.

32. Riche, V., et al., *Investigations on OFDM Signal for Range Ambiguity Suppression in SAR Configuration*. Geoscience and Remote Sensing, IEEE Transactions on, 2013. **PP(99)**: p. 1-4.
33. Riche, V., et al. *OFDM signal design for range ambiguity suppression in SAR configuration*. in *Geoscience and Remote Sensing Symposium (IGARSS), 2012 IEEE International*. 2012.
34. Riche, V., et al. *Optimization of OFDM SAR signals for range ambiguity suppression*. in *Radar Conference (EuRAD), 2012 9th European*. 2012.
35. Wang, W.Q., *Mitigating Range Ambiguities in High-PRF SAR With OFDM Waveform Diversity*. Geoscience and Remote Sensing Letters, IEEE, 2013. **10(1)**: p. 101-105.
36. Akhtar, J. *Cancellation of range ambiguities with block coding techniques*. in *Radar Conference, 2009 IEEE*. 2009.
37. Jian, F., et al. *SAR range ambiguity suppression via sparse regularization*. in *Geoscience and Remote Sensing Symposium (IGARSS), 2012 IEEE International*. 2012.
38. Garmatyuk, D. and M. Brenneman. *Slow-time SAR signal processing for UWB OFDM radar system*. in *Radar Conference, 2010 IEEE*. 2010.
39. A Viterbi, A.J., *CDMA: principles of spread spectrum communication*. D 1995, C Redwood City, CA, USA: I Addison Wesley Longman Publishing Co., Inc.

VITAE

Name :Mohammed Dahiru Buhari

Nationality :Nigeria

Date of Birth :5/21/1984

Email :jobsforbuhari@yahoo.com

Address :KFUPM main Campus Bld. 807 Room 213

Academic Background :Received Bachelor of Engineering (B.Eng) degree in Electrical Electronics Engineering from Abubakar Tafawa Balewa University Bauchi, Nigeria. Joined King Fahd University of Petroleum and Minerals, Dhahran, Saudi Arabia in January, 2012 and obtained Master of Science (M.Sc) degree in Telecommunication Engineering from the department of Electrical Engineering in 2014.